Memoirs of the Faculty of Engineering, Nagoya University
Vol. 40, No. 2 (1988)

DEFORMATION AND FAILURE OF ROCKS UNDER "WEAK" CYCLIC LOADING AND INCREMENTAL ELASTO-PLASTICITY THEORY

YASUAKI ICHIKAWA, TAKASHI KYOYA, ÖMER AYDAN, KAZUHITO YOSHIKAWA, TOSHIKAZU KAWAMOTO and NAOHIKO TOKASHIKI*

Department of Geotechnical Engineering

(Received October 31, 1988)

Abstract

This paper presents the experimental and theoretical studies on deformation and failure behaviours of the typical weak and hard rocks for conventional triaxial tests under monotone and "weakly" cyclic loadings. These materials show the dilation characteristics at lower confining pressures and the brittle-ductile transition. We present a non-associated plasticity theory using a dilatancy function for plastic behaviour under monotone loading, and an extended multi-response theory to elasto-plastic behaviour under "weakly" cyclic loading. In these approaches, we treat only the strain hardening response of geomaterials as the material behaviour and do not apply them to the strain-softening response since the softening is a structural phenomenon rather than a material characteristic. We present the response functions by a Laplace trasformation. The response models are applied to simulate the behaviours of Oya-tuff under monotone loading with non-linear plastic response, and the behaviours of Funyu-tuff and granite under cyclic loading with non-linear elastic and plastic responses, respectively. We also describe a procedure for conventional triaxial tests of rock materials by a stiff testing machine, a closed measurement-analysis-system for a laboratory test performed by a microcomputer and a data banking system of rock triaxial tests.

* University of Ryukyu, Nishihara-cho, Okinawa, Japan

Contents

1. Introduction

It is well-known that, in general, the mechanical behaviour of geomaterials such as rock and soil shows a non-linear response, and a dilatant plastic deformational behaviour, associated with shearing under compressive loading. And the strain softening phenomenon is also observed for most rock materials in triaxial tests under lower confining pressures. To investigate deformational behaviour and failure of rocks under monotone and weakly cyclic loadings, a series of conventional triaxial tests were carried out on typical weak and hard rocks. Here, the "weakly" cyclic loading implies that the reloading path is same as the unloading one. We show the experimental results for Oya-tuff under monotone loading, and for

Funyu-tuff and granite under cyclic loading. These materials commonly show a transition from brittle or strain-softening behaviour to strain hardening or ductile behaviour, and are accompanied by a dilation behaviour at low confining pressures.

Based on the experimental results, we present two incremental elasto-plasticity theories which are applicable to non-linear plastic response under monotone loading, and to non-linear elastic and plastic response under cyclic loading, respectively. Generally, a number of elasto-plastic theories[1)-4)] are applied to geomaterials in order to describe their non-linear plastic behaviour, but it is also known that the incremental plasticity theory using flow theory includes several ambiguities when it is applied to dilatant materials. These ambiguities essentially are caused by the plastic flow theory, which requires a scalar potential function as a plastic potential, and defines the plastic strain by differentiating its potential function.

Rudnicki and Rice[5)] derived an incremental constitutive law for dilatant materials directly by adding a friction term to the Prandtl-Reuss' equation, and defined a dilatancy function as the ratio of volumetric plastic strain increment to the norm of deviatoric plastic strain increment, which then they imposed to Mises flow law. This is a simple procedure and physical meanings of the resulting constitutive relation become trivial. However, some basic features have not yet been fully discussed in terms of a yield function and a flow potential.

We have already proposed an incremental plasticity theory, called the multi-response theory which defines the plastic response functions both for the shearing and volumetric behaviour.[6)] This theory gives the complete solution for ambiguities involved in the flow theory. It was applied for some rock materials under monotone loading, and comprehensive results were shown.

In this study, we propose an alternative incremental plasticity theory which is a non-associated plasticity model using a dilatancy function for the plastic behaviour of geomaterials under monotone loading. The constitutive law is derived by introducing the dilatancy function under the assumption of a non-associated flow law with Drucker-Prager's yield condition and isotropic hardening rule. The plastic response is represented by using the Laplace transformations by treating the responses as monotone.

As for the elastic-plastic behaviour of geomaterials under cyclic loading, many theories[7)-11)] have been proposed within the framework of flow theory. However, these models still involve on versality in describing the shear and volumetric responses independently. We have presented the extended multi-response theory to non-linear elastic and plastic behaviours of geomaterials under cyclic loading[12)]. In the theory, the elastic and the plastic response functions should be defined for the shearing and volumetric behaviours, because most rocks exhibit the plastic strain at the very beginning stage of cyclic loading, and the elastic response is also non-linear. These response functions are also represented by Laplace transformation since the monotone response was assumed. As an example of application, we present the results of granite under cyclic loading.

We also describe a procedure for the conventional triaxial test of rock materials, and a measurement system of experimental data by a microcomputer to determine parameters of constitutive models based on proposed incremental plasticity theory. In addition we have developed a data bank system to store the actual data gathered during triaxial tests.

2. Triaxial Tests for Rock

2. 1. Testing apparatus; high stiff testing machine

To investigate the deformation and failure characteristics of brittle materials such as

rock, the stiffness of testing machine must be sufficiently increased to control instantaneous deformations of specimens in compression tests. Usually, most testing machines of the stiff type employ a closed-loop servo-controlled oil pressure system. This system requires the instantaneous control of oil pressure at the failure of specimen, and it has a disadvantage because of the decreased stiffness of machine due to the compressibility of oil. Therefore, we have newly developed a high stiff testing machine which controls the displacement rate of specimen by the mechanical servo-control system.[13)]

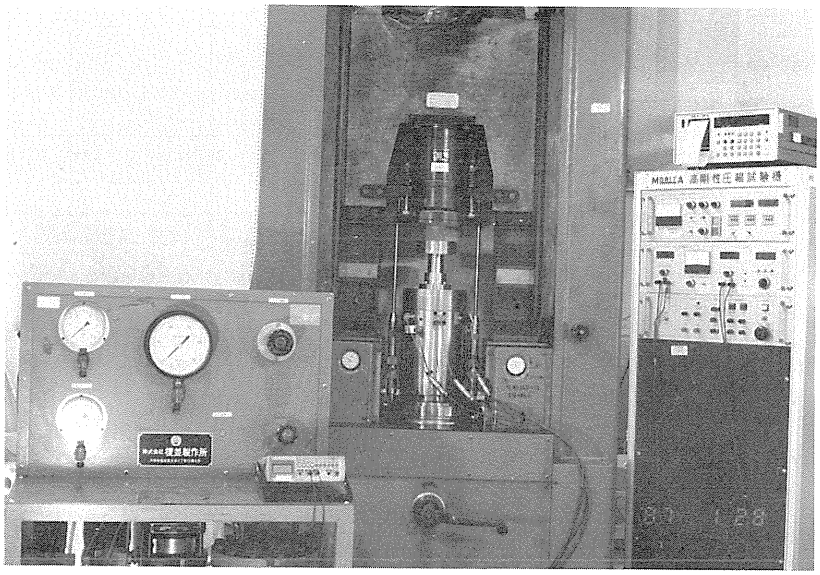

Fig. 2. 1. Overview of high stiff testing machine

The high stiff testing machine is shown in Fig. 2. 1. This testing machine is developed to do tests on rock-like materials under monotonic or cyclic triaxial loading conditions, and has following special features; 1) The overall stiffness of the machine is about 3.12×10^3 kN/mm, and the stiffness is increased by employing a stiff loading frame and by arranging two steel blocky columns parallel to the axis of the specimen. 2) Using the mechanical servo-control system with a satisfactory stiffness of the machine, the deformation characteristics including the pre-failure and post-failure behaviour of rocks such as the strain hardening and the strain softening can be easily obtained. 3) The machine is capable of controlling either deformation or load, and the loading and unloading points during cyclic loading can be set in both displacement and load. 4) The loading with an arbitrary deformation rate may also be applied by using a variable deformation rate controlling unit.

This testing apparatus consists of a loading frame, a hydraulic pump unit for the loading ram, a control equipment for displacement rate, and a measurement unit. The control system of the testing machine is shown in Fig. 2. 2. The control of displacement

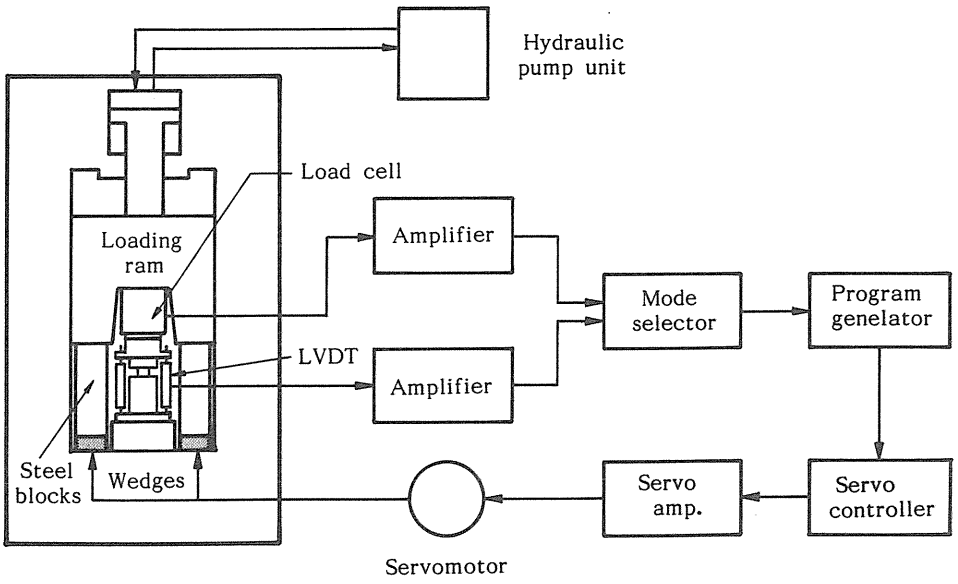

Fig. 2. 2. Schematic diagram of control system of high stiff testing machine

Table 2. 1. Specifications of high-stiff testing machine

Stiffness		Load cell Steel columns Overall	6.45 MN/mm 6.05 MN/mm 3.12 MN/mm
Measurement apparatus	Load cell	Capacity Measurement error Output voltage	1 MN ±1 % 1V full scale
	Displacement transducers (LVDT)	Stroke of displacement Measurement error Output voltage	5 mm ±1 % 0.06V full scale
Controlling apparatus	Print motor	Loading capacity Loading range Defromation rate	0.2 KW 0.2, 0.5, 1 MN 0.01 – 1 mm
	Loading control unit	Capable of controlling deformation rate and applied load rate Capable of programmed control of monotone and cyclic loading	
Hydraulic pump unit loading rams		oil pressure (up to) oil flow rate	20 MPa 1.5 l/min

of the specimen during a compression test is performed as follows: First, the loading is simultaneously applied to the specimen and the columns parallel to the specimen using the loading ram activated by oil pressure. Then, the loading on specimen is applied by vertical movement of the top of the columns, which can be adjusted vertically by the horizontal movement of two steel wedges installed under the columns using a direct current servo-motor. The direct current servo-motor, so called print motor, is controlled by the desired displacement or loading rate set by the program generator in the control equipment of the machine. Two linear variable differential transducers (LVDT) are attached between the top and the bottom loading plates to measure axial displacement of a specimen, and to control the vertical movement of the columns. Also, a stiff vertical load transducer is attached to the loading ram to measure the applied load.

Specifications of the testing machine are shown in Table 2. 1. The vertical load transducer is 1 MN capacity and has a stiffness of 6.45×10^3 kN/mm. The stroke of the vertical movement transducer is a maximum of 5 mm. The speed of the vertical movement of the loading head ranges from 0.01 to 1 mm/min.

2. 2. *Deformation measuring instruments*

The conventional triaxial test is used to obtain deformation and failure characteristics of geomaterials. Appropriate theoretical descriptions of continuum mechanics can be established by inserting these experimental results. To support analyses based on proposed incremental plasticity theory, it is necessary to develop a triaxial test which allows the measurement of the parameters needed for its analytical model. It is important, therefore, to measure closely the axial strain and the volumetric strain of rock specimens in compression test to specify the parameters in the proposed elasto-plastic model. Usually, it is difficult to measure the axial and the volumetic strain for rocks under triaxial stress state. Therefore, we developed a triaxial cell and a deformation measurement system which consists of two linear variable differential transducers and three gauges of ring type. These measurement apparatus are set on a specimen in the triaxial cell. We have performed monotonic triaxial tests for many rocks by using the triaxial cell and the measurement system of axial and volumetric strain. This test procedure is also adapted to cyclic loading conditions.

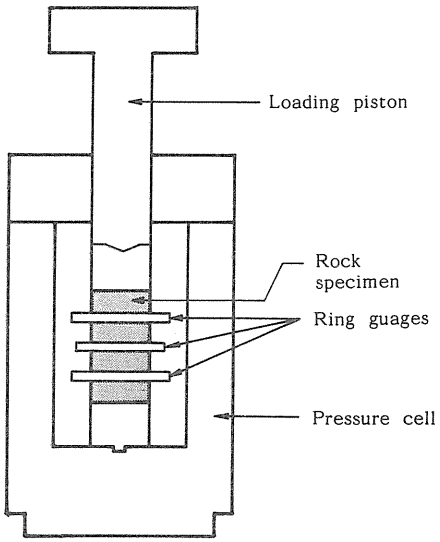

Fig. 2. 3. Setting of rock specimen and pressure cell for triaxial test

A triaxial cell, designed to accomodate measuring axial and volumetric strain of a specimen with dimensions of 50 mm in diameter and 100 mm in length, is illustrated in Fig. 2. 3. The cell has a confining pressure capacity of 19.6 MPa, and can be used in monotonic and cyclic compression tests. A specimen with the attached measurement apparatus can be easily mounted in the cell which is designed to connect the measurement apparatus set in the cell with a strain amplifier. To measure the distributions of radial displacements of a specimen, newly developed three ring gauges

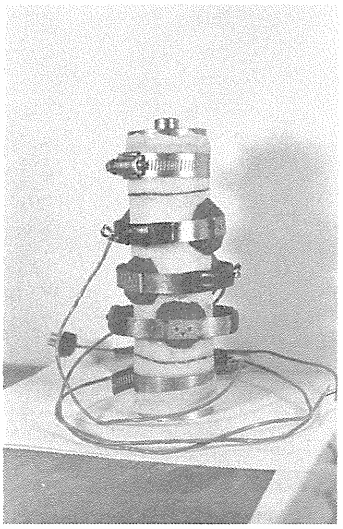

Fig. 2. 4. (a) Ring gauges

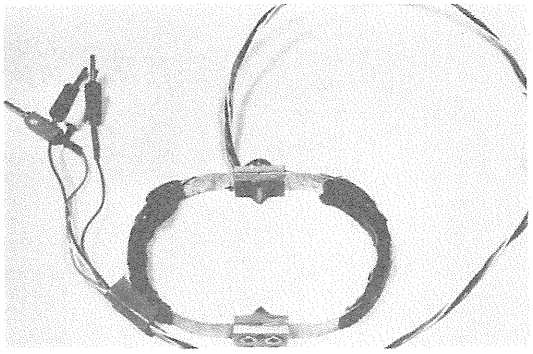

Fig. 2. 4. (b) Ring gauges

are attached to the specimen at the top, in the middle and at the bottom of the specimen with an angle of 120-degree respectively, as shown in Fig. 2. 4 (b). The ring gauge is an ellipsoid, of which the apsides is instrumented with four strain gauges (Fig. 2. 4 (a)); each strain gauge is covered by an oilproof coating. The edges of the ring gauge clip the side of the specimen.The gauges are attached to rock directly at locations where the rubber sleeve had slits. These slits, later on, are sealed with latex following the setting gauges in order to prevent oil from permeating into the rock during tests.

In early series of monotonic triaxial tests, the axial strain was obtained from measured axial displacements between the loading plates of the machine by using differential transducers outside of the cell. This measurement technique has a disadvantage that the measured displacement does not exactly correspond to the displacement of a specimen itself. Therefore, we also developed a system of measuring axial displacement of a specimen, directly. To measure the axial

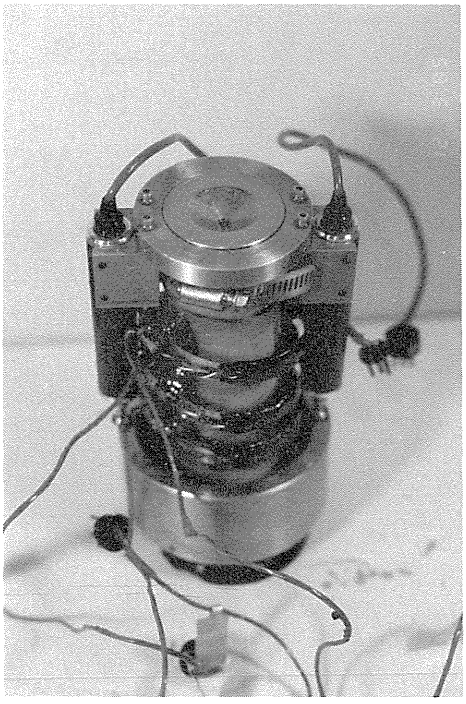

Fig. 2. 5. Newly developed ring gauges and LVDT system

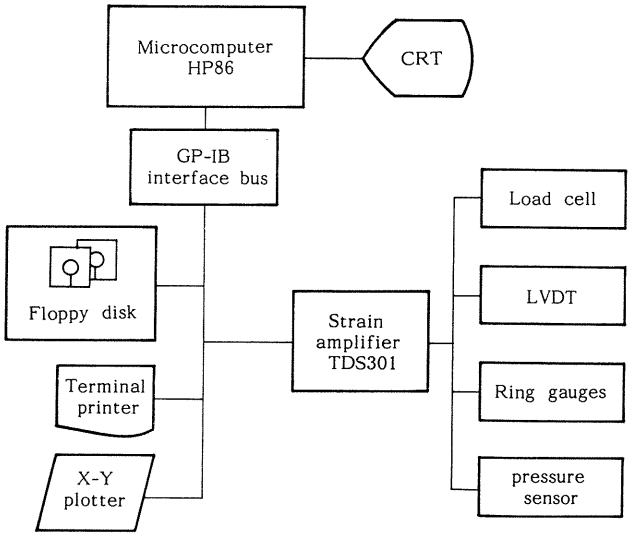

Fig. 2. 6. Schematic diagram of measurement system

Fig. 2. 7. Microcomputer used in measurements and analysis

displacement of a specimen, two linear variable differential transducers (deflection of 10 mm of travel) are attached to the top and bottom loading platens by an annular attachments, as shown in Fig. 2. 5. Thus, a more accurate measurement of the axial displacement of a specimen can be made using this new measurement apparatus.

2. 3. Data gathering system

In the incremental plasticity theory, to be presented next sections, the response functions of elasticity and plasticity are resolved by a multiple Laplace transformation. These response functions are determined from experimental data using a method of spectrum approximation. We developed a closed measurement-analysis system with the use of a microcomputer to gather the experimental data automatically, and to determine the plasticity spectrum and the elastic, the plastic response functions from the obtained data in conventional triaxial tests on rocks.

The typical block diagram of the experimental measurement system for laboratory test is shown in Fig. 2. 6. The measurement system is consisted of a microcomputer, a display (CRT), a floppy disk unit with two floppy disk drives, a terminal printer, a graphics plotter and a digital strain amplifier. These external devices are connected to the microcomputer by GP-IB interface bus (IEEE-488 bus). The microcomputer used in the system is HP-86 model, previously, or HP-9816 model, recently, of Hewlett-Packard (Fig. 2. 7). These microcomputers are used for both the measurement of experimental data during tests and the analyses of the measured data. In testing, this microcomputer is used to control the strain amplifier and other external devices, and to store the measured data in floppy disks.

Together with the microcomputer, a digital strain amplifier, TDS-301 (TML, Tokyo

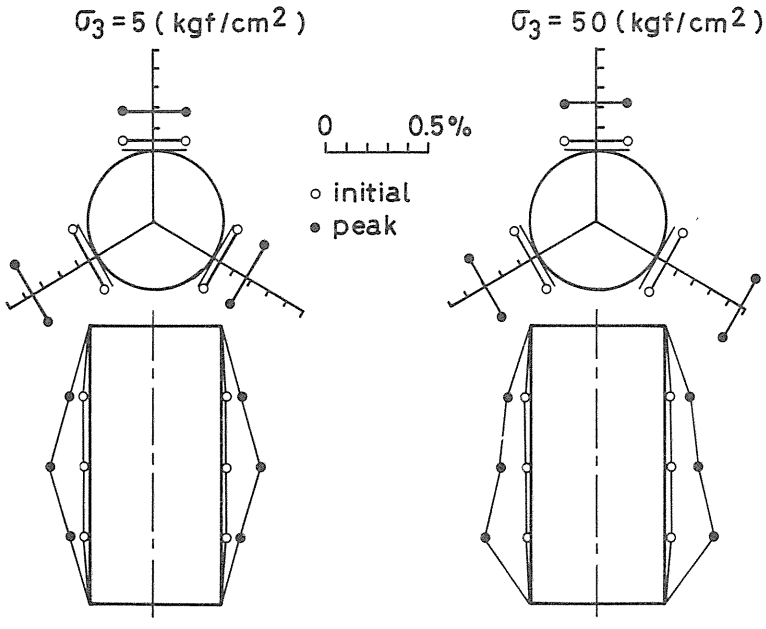

Fig. 2. 8. Typical lateral displacement distributions measured by ring gauges

Sokki Kenkyujo) is also used for the measurement of experimental data. For an automatic data gathering system, the TDS-301 can be programmable via the GP-IB. The ten channels are available for measurements. In the tests, the six channels are used for the measurements of load, displacement and confining pressure. The applied load is measured by a load cell, the axial displacement by two LVDT, the lateral displacement by three ring gauges, and the confining pressure by a pressure transducer. Fig. 2. 8 shows a typical lateral displacement distribution measured by ring gauges. The data for initial testing conditions and the calibration data of transducers are inputed and stored in the floppy disk before starting the test. After the initial set of transducers, the microcomputer activates the strain amplifier by sending a trigger starting command, and measurements are made at regular intervals as desired. The data taken by the TDS-301 is send to the microcomputer through the GP-IB. In real time, the microcomputer displays the obtained the axial stress-strain curve in the CRT and stores the measured data in a floppy disk with appropriate formats.

2. 4. Specimens

To investigate the inelastic behaviour of rock, we have performed monotonic and cyclic triaxial tests on many weak and hard rocks. The deformation modulus and the compressive strength in uniaxial tests are given in Table 2. 2. In the test, sedimentary porous rocks, called the Oya-tuff, the Funyu-tuff and the Ryukyu-limestone are chosen as weak rocks, and granite and rhyolite as hard rocks.

Table 2. 2. Strengths and elastic modulus of specimens in uniaxial tests

Rock type	Compressive strength (MPa)	Elastic modulus (MPa)
Oya-tuff	12	2300
Funyu-tuff	22	2800
Ryukyu limestone	13	7200
Omotani ryorite	205	41400
Granite	130	29200

The shape of the specimen is a cylinder to avoid 'edge' effects. The specimen is 50 mm in diameter and 100 mm in length, and a length/diameter ratio of which is 2.0. The specimen ends are cut parallel to each other and ground to be smooth. Moisture content of the specimen is controlled to obtain naturally dried condition.

2. 5. Procedures of triaxial tests

The incremental plasticity theory defines the plastic response functions both in the shearing and volumetric behaviours after the onset of plastic yielding. The material treated here is assumed to be isotropic and hydrostatically symmetric. This implies that the response is associated with by the relation between the volumetric stress, the deviatoric stress and the volumetric plastic strain, the deviatoric plastic strain. Therefore, the conventional triaxial test using cylindrical specimens is useful to obtain the plastic response of rock materials.

It is known that the deformation behaviour of rock materials shows nonlinear elastic

response as well as a nonlinear plastic response under applied loads. The incremental plasticity theory gives the plastic response by assuming a linear elastic response of rock materials. The extended incremental elasto-plasticity theory discribes the nonlinear elastic and plastic response of rock materials. Thus, two types of the conventional triaxial test on rock materials are performed. The monotonic triaxial tests are carried out to get the linear elastic and plastic response model. Also, the weakly cyclic triaxial tests are conducted to obtain the nonlinear elastic and plastic response model. Also, the weakly cyclic triaxial tests are conducted to obtain the nonlinear elastic and plastic response model.

The all tests are carried out at several stages of confining pressure from 0 to 10 MPa. The method of testing for both monotonic and cyclic test is as follows: firstly the predetermined constant confining pressure is applied to the specimen. Then, the axial load is applied at a constant deformation rate of 0.1 mm/min (0.1 %/min) by the displacement control system of the stiff testing machine. The monotonic loading tests are conducted by applying the axial load without unloading until the peak strength of the material is exceeded (achieved). In the cyclic test, the cyclic loading is started by loading to the required confining pressure, because the volumetric strain needs to be separated into elastic and plastic components to obtain the nonlinear elastic and plastic response of rock materials. The returning points of unloading during cyclic test are set up at regular intervals of strain level by the deformation control system of stiff testing machine, automatically.

The experimental data during tests are gathered by the data gathering system using a microcomputer, and stored in floppy disks as described in the previous section.

2. 6. *Data banking system for rock triaxial tests*

To measure the deformational and failure characteristics of geomaterials many triaxial tests are usually undertaken. Once tests have been used for a certain purpose, the use of these results from another point of view is usually rare. Nevertheless, the tests results on the deformational and failure characteristics may be re-examined from different view points and their constitutive equations can be re-evaluated. Thus, a system to store these tests results and to process for the given purpose is necessary in order to make the effective use of the results. There are some recent attempts to make use of the existing laboratory and in-situ test results obtained for the design of geotechnical engineering structures in association with the use of underground space. Accordingly, by creating a data banking system for triaxial tests in laboratory and incorporating with the future rock mass data base system will lead a data base system with a large amount of accumulated information which is expected to lend itself to further developments. From this point of

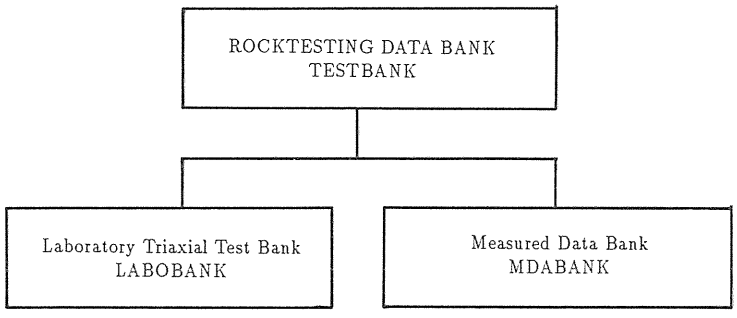

Fig. 2. 9. The structure of data banking system

view, we have developed a data processing measurement system for the triaxial tests in laboratory and have been attempting to develop a data banking system for the existing and future tests results using a personal computer as described previously.

We name the data banking system "TESTBANK", the structure of which is shown in Fig. 2. 9. The structure of the system consists of two data banking sub-systems; "LABOBANK" and "MDABANK". As shown in Table 2. 3, the "LABOBANK" system consists of 20 items of information on rock type, test number, physical property names, testing procedures and storage locations (files) of data. On the other hand, the "MDA-BANK" system store the actually measured results of triaxial tests and test conditions and consists of 21 items of information as shown in Table 2. 4. The "TESTBANK" system makes use of a personal computer and the mass storage facilities of a large scale computer. The "LABOBANK" system operates on the personal computer and is programmed in a soft wear data bank programming language available on the market. The main purpose of the "MDABANK" system is designed to store a large amount of experimental data by using the mass storage facilities of the large scale computer. The "TESTBANK" system is connected with the large scale computer, and is accessed to the mass storage facilities through the "MDABANK" sub-system on the basis of information required from the "LABOBANK" sub-system.

Table 2. 3. Data file items (LABOBANK)

Specification	No	Data File Items
Test	1	test location
	2	test date (Year/Month/Day)
	3	test number
Specimen	4	rock type
	5	sampling Location
Test Details	6	sample number
	7	shape
	8	dimensions
	9	accuracy of sample preparation
Physical Properties	10	unit weit γ_t (g/cm^3)
	11	density ρ
	12	moisture content ω (%)
	13	void rato e
	14	porosity n (%)
	15	degree of saturation S_r
Testing procedures	16	loading condition
	17	controlling method
	18	loading accuracy
	19	confining pressure C_pMPa
Storage Address of test data	20	Test data storage code

Table 2. 4. Data file items (MDABANK)

Specification	No	Data File Item
Test conditions	1	test number
	2	sample number
	3	test date (Year/Month/Day)
	4	diameter
	5	height
	6	confining pressure
	7	ring gauge number 1
	8	ring gauge number 2
	9	ring gauge number 3
	10	coefficient of load cell
	11	coefficient of LDVT 1
	12	coefficient of LDVT 2
	13	coefficient of pressuremeter
	14	initializing value (Load)
	15	initializing value (LDVT 1)
	16	initializing value (LDVT 2)
	17	initializing value (Ring gauge 1)
	18	initializing value (Ring gauge 2)
	19	initializing value (Ring gauge 3)
	20	initializing value (Pressuremeter)
Number of Data	21	number of data for load, displacements pressuremeter etc.

3. Deformation and Failure Characteristics of Several Rocks

To investigate the deformation behaviour of rocks from a viewpoint of the incremental plasticity theory, we have performed monotonic and cyclic triaxial tests on many rocks. We here show the results of triaxial tests on five rock types. The rocks tested and the main features of their stress-strain characteristics and volumetric strain response are described below. Plastic deformation characteristics obtained from monotonic and cyclic tests are described in Chapter 5.

3. 1. Sedimentary rocks: Oya-tuff and Funyu-tuff and Ryukyu Limestone

Three types of sedimentary porous rocks, called Oya-tuff and Funyu-tuff and Ryukyu limestone were used in tests and their physical properties are given in Table 3. 1. The monotonic triaxial tests for Oya-tuff were carried out at various confining pressures. Measured stress-strain curves for Oya-tuff specimens are shown in Fig. 3. 1. Clearly, the stress-strain curves show a transition from brittle behaviour to ductile behaviour, which is seen at the confining pressure of 4.5 MPa. Volumetric strain-differential stress curves is also accompanied by dilation at lower confining pressures of 4.5 MPa (Fig. 3.2).

A series of triaxial tests on Ryukyu limestone, which is an organic type sedimentary rock, were carried out under monotone loading conditions. Figs. 3. 3 and 3. 4 show the

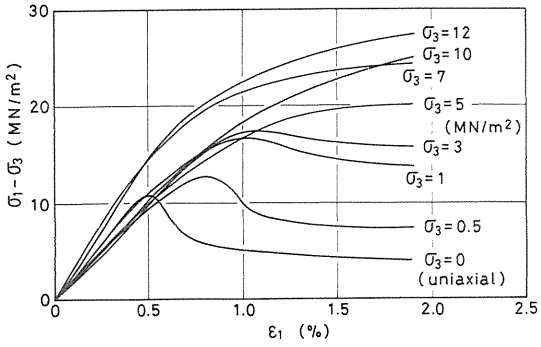

Fig. 3. 1. Differential stress-axial strain curves for various confining pressures (Oya-tuff)

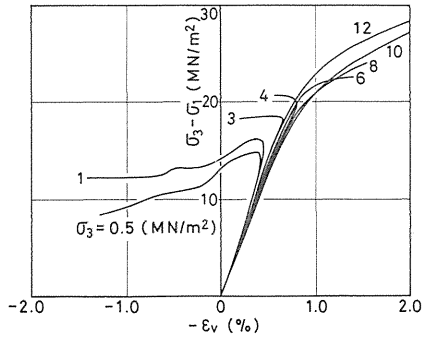

Fig. 3. 2. Differential stress-volumetric strain curves for various confining pressures (Oya-tuff)

Table 3. 1. Physical properties of specimens

Physical properties		Oya-tuff	Funyu-tuff	Ryukyu limestone	Omotani rhyolite	Granite
unit weight	r_t (g/cm^3)	1.56	1.67	2.21	1.93	1.88
moisture content	ω (%)	5.20	6.59	—	4.57	3.74
void ratio	e	0.61	0.33	—	0.34	0.22
porosity	n (%)	37.7	24.9	—	25.3	18.0
degree of saturation	Sr (%)	—	41.3	—	34.6	37.6

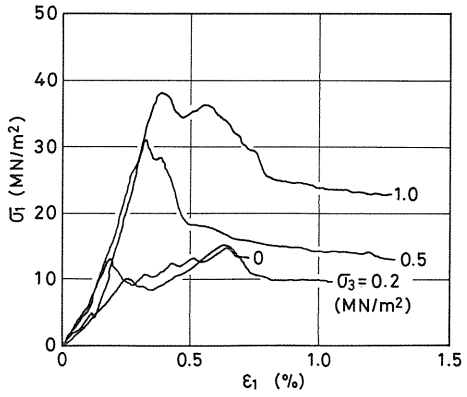

Fig. 3. 3. Axial stress-axial strain curves for various confining pressures (Ryukyu limestone)

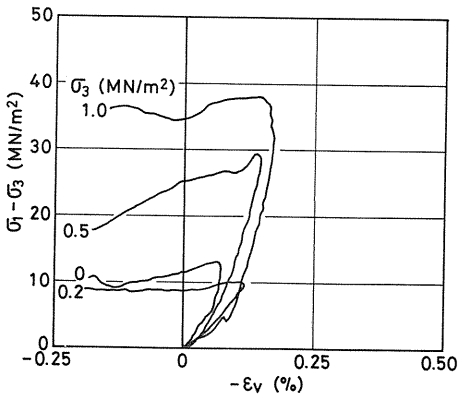

Fig. 3. 4. Axial stress-volumetric strain curves for various confining pressures (Ryukyu limestone)

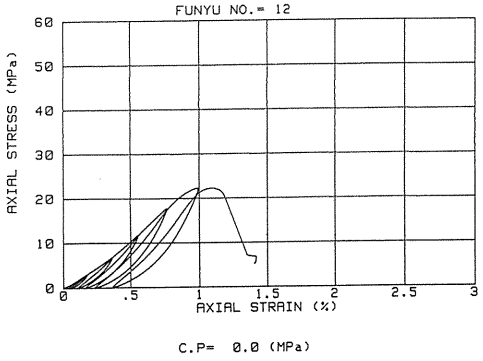

Fig. 3. 5. Response of Funyu-tuff under cyclic loading (0.0 MPa)

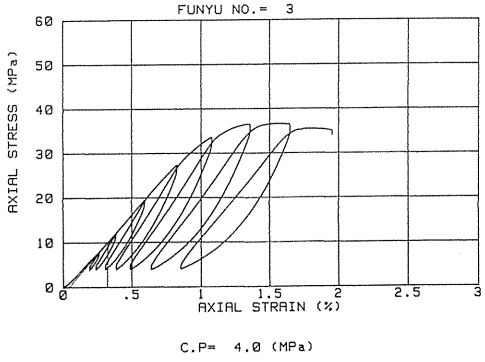

Fig. 3. 6. Response of Funyu-tuff under cyclic loading (4.0 MPa)

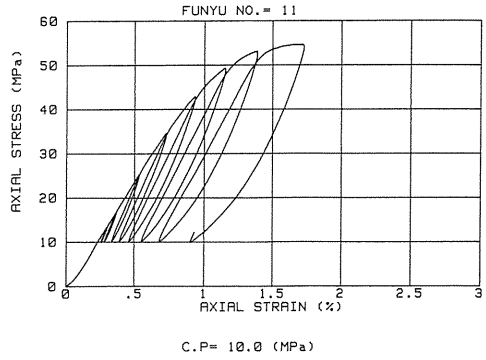

Fig. 3. 7. Response of Funyu-tuff under cyclic loading (10.0 MPa)

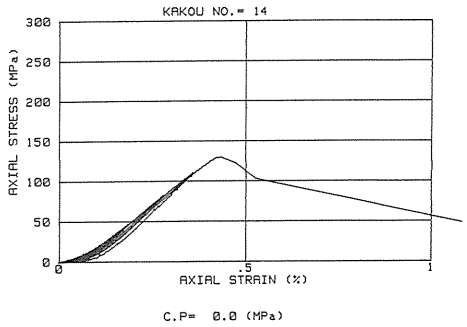

Fig. 3. 8. Response of granite under cyclic loading (0.0 MPa)

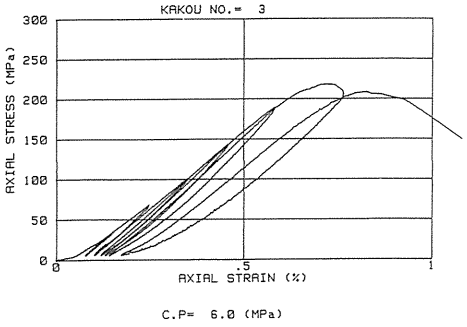

Fig. 3. 9. Response of granite under cyclic loading (6.0 MPa)

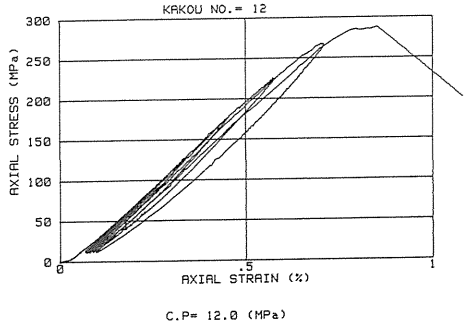

Fig. 3. 10. Response of Funyu-tuff under cyclic loading (12.0 MPa)

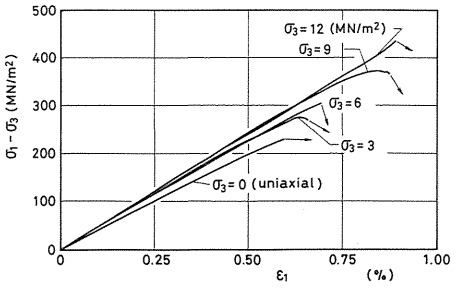

Fig. 3. 11. Differential stress–axial strain curves for various confining pressures (Omotani-rhyolite)

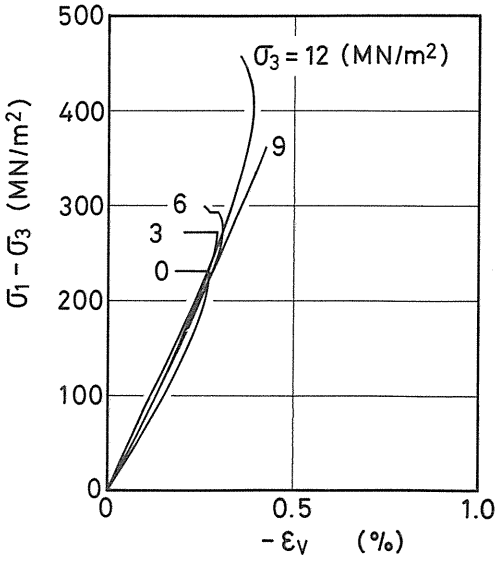

Fig. 3. 12. Differential stress-volumetric strain curves for various confining pressures (Omotani-rhyolite)

axial stress–axial strain curves and deviatoric stress–volumetric strain curves. For the applied range of confining pressures, this rock shows a brittle and dilatant behaviour.

A series of triaxial cyclic tests on Funyu-tuff was carried out in order to investigate nonlinear elastic and plastic deformation at some lower confining pressures. The typical results of cyclic tests on Funyu-tuff are presented in Figs. 3. 5 to 3. 7. The typical figures includes axial stress–axial strain curves, axial stress–lateral strain curves and volumetric stress–volumetric strain curves at confining pressures of 0, 4.0 and 10.0 MPa. In Fig. 3. 5, the envelop curves which are the upper loading surfaces of the stress–strain curves, are coincided with the stress–strain curves during monotonically loading. The envelop curves of the stress–strain relations show a transition from strain softening behaviour to strain hardening behaviour. The volumetric stress–volumetric strain curves show reduced dilation at higher confining pressures (Fig. 3. 7).

3. 2. Igneous Rocks: Granite and Omotani Rhyolite

In order to study the cyclic deformation behaviour of hard rocks, cyclic triaxial tests on granite were performed at various confining pressures between 0 and 12 MPa. The typical results of the tests at confining pressures of 0, 6.0 and 12.0 MPa are shown in Fig. 3. 8 to 3. 10. The envelop curves of stress–strain relations in Fig. 3. 8 are also coincided with the stress–strain curves obtained in tests of monotonically loading. It is noted that typically, the plastic strain level at peak strength of the stress–strain relation of granite (Fig. 3. 8) is relatively lower than the plastic strain level at peak strength of the stress–strain relation of Funyu-tuff (Fig. 3.5). The small dilation is occured at lower confining pressures as seen in Fig. 3. 10.

A series of triaxial tests on Omotani-rhyolite, which is a typical extrusive type of igneous rock, were carried out under monotone loading conditions. Figs. 3. 11 and 3. 12 show the axial stress–axial strain curves and deviatoric stress–volumetric strain curves. For the applied range of confining pressures, this rock shows a brittle and dilatant behaviour.

4. Incremental Elasto-Plasticity Theory for Geomaterials

The incremental plasticity theory based on the flow rule is commonly used in modeling nonlinear plastic behaviour of geomaterials. The flow theory is not appropriate for estimating dilatancy effect of geomaterials, since the flow theory requires a scalar potential function as a plastic potential in the flow equation. Moreover, it is difficult to specify a plastic potential function, directly, if the non-asssociated flow rule is used. Rudnicki and Rice, and Nemat-Nasser suggested to introduce a dilatancy factor instead of the plastic potential function. However, some basic features have not yet been fully discussed in terms of a yield function and a flow potential.

We here present three incremental plasticity theories; i-) The flow theory, ii-) The multi-response theory, and iii-) The non-associated flow theory with a dilatancy function. The section devoted to the flow theory is a summary of the fundamentals of the classical theory of plasticity. The multi-response theory is a new approach to describe the elasto-plastic behaviour of geomaterials. The third theory, though is based on the flow theory of non-associated type, introduce a dilatancy function to represent the dilatant behaviour of geomaterials. Responses and dilatancy functions in the latter approaches are identified by a Laplace transformation method. Spectral points of these functions

are directly specified from experimental data. The models are applied to study the plastic response of several rocks in the latter sections.

As the volumetric deformation of geomaterials occurs independently of the shear deformation, the geomaterials can be said to be a general material as compared with the metals. Therefore, it is difficult to treat this kind of materials using the flow theory, more explicitly, the scalar potential theory. To solve the insufficiency of the flow theory, the multi-response theory has been proposed. Nevertheless, this theory requires very accurate measurements in order to determine the volumetric and deviatoric responses. In addition to this, a non-associated flow theory employing a dilatancy function has been presented. The responses and dilatancy functions are represented through the Laplace transformation. Then these model are applied to simulate the behaviour of several rocks under monotone and cyclic loadings. For the proposed theories, a procedure for triaxial tests of geomaterials by a stiff testing machine, a closed-measurement-analysis system for a laboratory test and a data bank system of rock triaxial test are described.

4. 1. Notations and terminologies

(Stress)

σ	: stress tensor
$\bar{\sigma}=tr(\sigma)I^{\sigma}/3$	: mean or volumetric stress tensor
$\bar{\sigma}=tr(\sigma)/\sqrt{3}$	: mean stress
$I^{\sigma}/3$	: unit tensor in the stress space
$s=\sigma-\bar{\sigma}$	: deviatoric (or shear) stress tensor
$s=\|\|s\|\|=(s\cdot s)^{1/2}$	: norm of the deviatoric stress tensor
$\theta^{\sigma}=\frac{1}{3}\cos^{-1}\{3\sqrt{3}\,J_3^{\sigma}/2(J_2^{\sigma})^{3/2}\}$	: stress Lode angle
$I_1^{\sigma}=tr(\sigma)$	: first invariant of the stress tensor
$J_2^{\sigma}=s\cdot s/2$	: second invariant of the deviatoric stress
$J_3^{\sigma}=det(s)$	: third invariant of the deviatoric stress

(Strain)

ε	: strain tensor
$\bar{\varepsilon}=tr(\varepsilon)I^{\varepsilon}/3$	: mean (or volumetric) strain tensor
$\bar{\varepsilon}=tr(\varepsilon)/\sqrt{3}$	: norm of strain tensor
I^{ε}	: unit tensor in the strain space
$e=\varepsilon-\bar{\varepsilon}$	: deviatoric (or shear) strain tensor
$e=\|\|e\|\|=(e\cdot e)^{1/2}$	: norm of the deviatoric strain tensor
$\theta^{\varepsilon}=\frac{1}{3}\cos^{-1}\{3\sqrt{3}\,J_3^{\varepsilon}/2(J_2^{\varepsilon})^{3/2}\}$	: strain Lode angle
$I_1^{\varepsilon}=tr(\varepsilon)$	: first invariant of the strain tensor
$J_2^{\varepsilon}=e\cdot e/2$	: second invariant of the deviatoric strain
$J_3^{\varepsilon}=det(e)$	: third invariant of the deviatoric strain

We here assume a straight unloading and reloading path (show as a solid line in Fig. 4. 1), and the strain ε is directly separated into elastic and plastic components:

$$\varepsilon=\varepsilon^{e}+\varepsilon^{p} \tag{1}$$

In the incremental form, it is written as

$$d\varepsilon=d\varepsilon^{e}+d\varepsilon^{p} \tag{2}$$

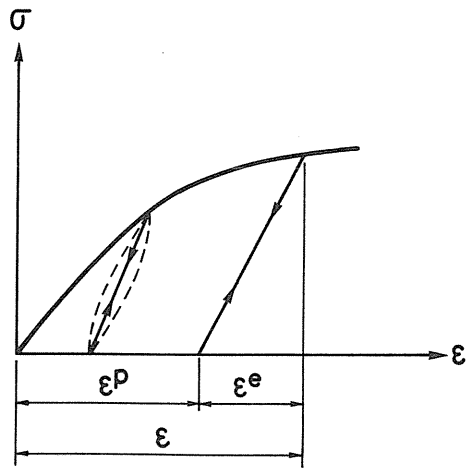

Fig. 4. 1. Definition of strains
(one-dimensional case)

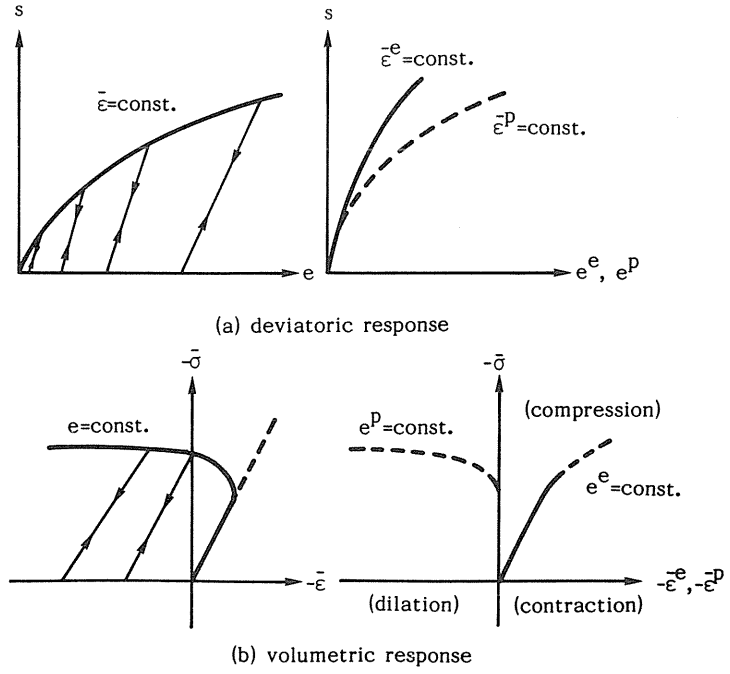

Fig. 4. 2. Schematic diagram of elasto-plastic response of dilatant materials

The elastic and the plastic responses are composed of the deviatoric and mean component, respectively. Thus, we obtain responses of dilatant materials as shown in Fig. 4. 2.

When the material is isotropic, the relation between stress and strain is independent of the coordinate system. In other words, the relation can be written in terms of mean and deviatoric components and the Lode angle. Herein, the relation between mean and deviatoric components will be treated. As such materials gives a symmetric response with respect to the hydrostatic axis $\sigma_1=\sigma_2=\sigma_3$, it will be called hydrostatically symmetric materials. This is a sufficient assumption when we consider the cylindrical specimens used in triaxial tests in laboratory.

In the following sections, we will be mainly concerned with rock-like materials, and present the flow theory and multi response theory. We will treat the strain-hardening response up to peak strength only not the strain softening response as we regard the softening behaviour as a structural phenomenon rather than a material characteristic.

4. 2. Flow theory for monotone loading

4. 2. 1. Yield function and hardening law

The surfaces of the initial and subsequent yieldings are generally given by:

$$f(\sigma,\ \varkappa)=0 \tag{3}$$

Hardening parameter $\varkappa$ representing the internal friction coefficient is written as

$$\varkappa=W^p=\int \sigma\cdot d\varepsilon^p \qquad \text{: Work hardening} \tag{4}$$

or

$$\varkappa=\int ||d\varepsilon^p|| \qquad \text{: Strain hardening} \tag{5}$$

Depending upon the introduced form of the friction coefficient, the yield function $f(\sigma,\ \varkappa)$ are usually written in the following forms:

$$f(\sigma,\ \varkappa)=f_I(\sigma)-K(\varkappa) \quad \text{: Isotropic hardening} \tag{6}$$

$$f(\sigma,\ \varkappa)=f_I(\sigma-\alpha(\varkappa)) \quad \text{: Kinematic hardening} \tag{7}$$

$$f(\sigma,\ \varkappa)=f_I(\sigma-\alpha(\varkappa))-f_2(\varkappa) \quad \text{: Anisotropic hardening} \tag{8}$$

$$d\alpha=c\,d\varepsilon^p \qquad \text{: Prager Type}$$

$$d\alpha=c(\sigma-\alpha)||d\varepsilon^p|| \qquad \text{: Ziegler Type}$$

There are various yield functions proposed, based upon the experimental data, in which the terms associated with stress differ from one yield criterion to another. We give some of them for $f_1(\sigma)$ of isotropic hardening model (Eqn. 6) as examples:

$f_1(\sigma) = \sqrt{J_2^\sigma}$: Mises

$f_1(\sigma) = \sqrt{J_2} + \alpha I_1^\sigma$: Drucker-Prager

$f_1(\sigma) = |\sigma_1 - \sigma_3|$: Tresca

$\sigma_1 \geq \sigma_2 \geq \sigma_3$: principal stresses

$f_1(\sigma) = \pm 1/2(\sigma_1 - \sigma_3)$

$+1/2(\sigma_1 + \sigma_3)\sin\phi - c\cos\phi$: Mohr-Coulomb

ϕ : Friction angle c : cohesion

$f_1(\sigma) = (I_1^\sigma)^3/I_3^\sigma$ Lada-Duncan

$I_3^\sigma = det(\sigma)$ third invariant of stress tensor

$f_1(\sigma) = I_1^\sigma I_2^\sigma / I_3^\sigma$: Matsuoka-Nakai

$f_1(\sigma) = \frac{\lambda-\varkappa}{1+e_0}\ln\frac{p}{p_0} + \frac{\lambda-\varkappa}{M(1+e_0)}\frac{q}{p}$: Cam-Clay model

$p = \sigma_{ij}/3 = \bar{\sigma}/\sqrt{3}$

$q = \sqrt{J_2^\sigma} = s/\sqrt{2}$

$p_0 =$ *Initial consolidation* e_0: Initial void ratio

M: the value of q/p at the limiting state

λ: Gradient of compression line e – ln p space

$\varkappa$: Gradient of unloading line e – ln p space

Of these, the cam-clay model is a typical example for isotropic hardening model of strain hardening type (Schofield and Wroth 1968).

$$K(\varepsilon^p) = \varepsilon_v^p = \varepsilon_{ij}^p$$

4. 2. 2. Consistency condition of Prager

For the material to continue behaving plasticly following the initial yielding, it must satisfy Eqn. (3). Thus,

$$f(\sigma + d\sigma,\ \varkappa + d\varkappa) = 0$$

As a result of this, one has

$$df = \frac{\partial f}{\partial \sigma} \cdot d\sigma + \frac{\partial f}{\partial \varkappa} d\varkappa = 0 \tag{9}$$

This is known as the consistency condition of Prager.

Inserting the work hardening law (4) in the consistency condition (9) yields

$$\frac{\partial f}{\partial \sigma} \cdot d\sigma + \frac{\partial f}{\partial \varkappa} \sigma \cdot d\varepsilon^p = 0 \tag{10}$$

On the other hand, subsituting the strain hardening law (5) in the consistency condition (9) gives

$$\frac{\partial f}{\partial \sigma} \cdot d\sigma + \frac{\partial f}{\partial \varkappa} \frac{\partial \varkappa}{\partial \varepsilon^p} \cdot d\varepsilon^p = 0 \tag{11}$$

The consistency condition of Prager has a very important role in the flow theory.

When the flow rule is subsituted in Eqn. (10) or Eqn. (11), it will be seen that this expression establishes a relation between the stress and strain increments. It is not wrong to say that the consistency condition of Prager itself is an incremental law.

4. 2. 3. Incremental plasticity theory based on the flow law

Let us write plastic strain increment $d\varepsilon^p$ in terms of plastic potential g which is very well known as the flow law.

$$d\varepsilon^p=\lambda\frac{\partial g}{\partial\sigma} \tag{12}$$

The flow law (12) implies that the direction of plastic strain increment is normal to g=constant surfaces and it is coaxial with the stress σ. For hydrostatically symmetric materials, the followings can be said. Now, let us write

$$m=\frac{\partial s}{\partial s}=\frac{\partial s}{\partial\sigma}=\frac{s}{s},\quad n=\frac{\partial\bar{\sigma}}{\partial\bar{\sigma}}=\frac{\partial\bar{\sigma}}{\partial\sigma}=\frac{\bar{\sigma}}{\bar{\sigma}},\quad l=\frac{\partial\theta^\sigma}{\partial\sigma} \tag{13}$$

As m, n, l are orthogonal to each other, one has

$$\frac{\partial g}{\partial\sigma}=\frac{\partial g}{\partial s}m+\frac{\partial g}{\partial\sigma}n+\frac{\partial g}{\partial\theta^\sigma}l$$

Thus, plastic strain increment $d\varepsilon^p$ is coaxial with stress σ. (Note: the stability condition of Drucker) Drucker writes the condition for a stable behaviour of an elasto-plastic material as

$$W^p=\int(\sigma-\sigma_0)\cdot d\varepsilon^p\geq 0$$

where σ_0 is an arbitrary stress state satisfying the following condition

$$f(\sigma_0,\ \varkappa)<0$$

This expression can be rewritten in the local form or by writing $\sigma=\sigma_0+d\sigma$ as

$$(\sigma-\sigma_0)\cdot d\varepsilon^p\geq 0 \tag{14}$$

If the flow law (12) is subsituted in Eqn. (14), one has

$$d\sigma\cdot d\varepsilon^p\geq 0$$

If σ_0 is chosen arbitrarily, and the above condition required to be satisfied, then it is implied that $g=f$ (associated flow law) and the convexity of f. However, this is a very strong condition and when the associated flow theory is applied to geomaterials, the dilatancy (volumetric expansion associated with shearing) is overestimated. To overcome

this problem, it is necessary to introduce plastic response functions for deviatoric and volumetric components separately instead of using the flow law which is based on the scalar potential theory.

When the flow law is used, the constitutive law can be obtained as follows: Subsituting the flow law in the consistency condition of Prager (10) or Eqn. (11) yields

$$\lambda=\frac{1}{h}\frac{\partial f}{\partial \sigma}\cdot d\sigma \tag{15}$$

where h is the hardening coefficient and given by:

$$h=\begin{cases} -\dfrac{\partial f}{\partial W^p}\sigma\cdot\dfrac{\partial g}{\partial \sigma} & \text{work hardening} \\ -\dfrac{\partial f}{\partial \varkappa}\dfrac{\partial \varkappa}{\partial \varepsilon^p}\cdot\dfrac{\partial g}{\partial \sigma} & \text{strain hardening} \end{cases} \tag{16}$$

Resubstituting Eqn. (15) in the flow law gives

$$d\varepsilon^p=\frac{1}{h}\frac{\partial g}{\partial \sigma}\left(\frac{\partial f}{\partial \sigma}\cdot d\sigma\right)=\frac{1}{h}\left(\frac{\partial g}{\partial \sigma}\otimes\frac{\partial f}{\partial \sigma}\right)d\sigma \tag{17}$$

where $\otimes$ is the tensor product, but when $\partial g/\partial\sigma$, $\partial f/\partial\sigma$ are represented by vectors, this tensor product can be considered in the following form

$$\frac{\partial g}{\partial \sigma}\otimes\frac{\partial f}{\partial \sigma}\rightarrow\left\{\frac{\partial g}{\partial \sigma}\right\}\left\{\frac{\partial f}{\partial \sigma}\right\}^T \tag{18}$$

Denoting the left terms of Eqn. (17) by

$$\boldsymbol{C}^p=\frac{1}{h}\frac{\partial g}{\partial \sigma}\otimes\frac{\partial f}{\partial \sigma} \tag{19}$$

one has the following.

$$d\varepsilon^p=\boldsymbol{C}^p d\sigma \tag{20}$$

Eqn. (17) is called Melan's formula.

Since the plastic compliance $\boldsymbol{C}^p$ obtained using the flow law, given by Eqn. (19) is represented by the tensor product of two tensors of second order, its determinant becomes zero ($\det(\boldsymbol{C}^p)=0$) in the way it is considered in Eqn. (18). Also, it should be noted that when the eigen values of the matrix are considered, there is only one non-zero eigen value at most and, the other eigen values are all zero. Therefore, the inverse of $\boldsymbol{C}^p$ can not be obtained directly and the following technique is used to obtain the elasto-plastic constitutive tensor $\boldsymbol{C}^{ep}$. Taking the dot product of the both sides of the following by $\partial f/\partial\sigma$,

$$d\sigma = \boldsymbol{D}^e d\varepsilon^e = \boldsymbol{D}^e (d\varepsilon - d\varepsilon^p)$$

$$= \boldsymbol{D}^e d\varepsilon - \boldsymbol{D}^e \frac{1}{h} \frac{\partial g}{\partial \sigma} \left(\frac{\partial f}{\partial \sigma} \cdot d\sigma \right) \tag{21}$$

yields

$$\frac{\partial f}{\partial \sigma} \cdot d\sigma = \frac{\partial f}{\partial \sigma} \cdot \boldsymbol{D}^e d\varepsilon / \left\{ 1 + \frac{1}{h} \frac{\partial f}{\partial \sigma} \cdot \left(\boldsymbol{D}^e \frac{\partial g}{\partial \sigma} \right) \right\} \tag{22}$$

Since $\boldsymbol{D}^e$ is symmetric, Substituting Eqn. (21) into Eqn. (22) gives:

$$\boldsymbol{D}^{ep} = \boldsymbol{D}^e - \left(\boldsymbol{D}^e \frac{\partial g}{\partial \sigma} \right) \otimes \left(\boldsymbol{D}^e \frac{\partial f}{\partial \sigma} \right) / \left\{ h + \frac{\partial f}{\partial \sigma} \cdot \left(\boldsymbol{D}^e \frac{\partial g}{\partial \sigma} \right) \right\} \tag{23}$$

When the flow law is employed, the undefineteness of the determinant of the plastic compliance $\boldsymbol{C}^p$ has an important meaning. More specifically, when the strain increment is given as the derivative of a scalar potential function as in the case of flow law, the parameter determined freely is only one because of the scalarness of the potential function. As a result, it becomes impossible to determine the volumetric strain and deviatoric strain independently.

Next, we would like to show how to determine the hardening function h. For the sake of simplicity, we will herein consider the isotropic hardening model (6). From Eqn. (16), we have

$$h = \begin{cases} \dfrac{\partial K}{\partial W^p} \sigma \cdot \dfrac{\partial g}{\partial \sigma} & : \text{Work hardening} \\ \left[\dfrac{\partial K}{\partial \varkappa} \dfrac{\partial \varkappa}{\partial \varepsilon^p} \cdot \dfrac{\partial g}{\partial \sigma} \right] & : \text{Strain hardening} \end{cases} \tag{24}$$

The function $\phi(\chi)$ is a homogenous function of order m with respect to an arbitrary scalar t if it satisfies:

$$\phi(t\boldsymbol{x}) = t^m \phi(\boldsymbol{x})$$

Then, the following relation should hold (Euler's theorem)

$$\boldsymbol{x} \cdot \frac{\partial \phi}{\partial \boldsymbol{x}} = m\phi(\boldsymbol{x})$$

For example, Mises $f_1 = \sqrt{J_2^q}$ and Drucker-Prager $f_1 = \sqrt{J_2^q} + \alpha I_1^q$ yield criteria are the first order homogenous functions. Note that when the Drucker-Prager yield criterion is written in the following form,

$$f_1 = J_2^q + \alpha I_1^q$$

$f_1(\sigma)$, no longer, is a homogenous function of σ.

When the associated flow law $f=g$ is employed, and f is an m order homogenous function of σ, then the work hardening given by Eqn. (24) simply becomes

$$h=m\frac{\partial K}{\partial W^p}f_1 \tag{25}$$

This is the reason why the work hardening law is commonly employed. Let us define the effective stress as:

$$f_1(\sigma)=\sigma_e$$

and the effective strain increment to be determined from the following identity,

$$dW^p=\sigma\cdot d\varepsilon^p\equiv\sigma_e d\varepsilon_e^p \tag{26}$$

then, the hardening coefficient is obtained as

$$h=m\frac{\partial\sigma_e}{\partial\varepsilon_e^p} \tag{27}$$

In the case of metals without volumetric plastic deformation, the expression written below has a meaning,

$$\sigma\cdot d\varepsilon^p=s\,de^p+\bar{\sigma}\,d\bar{\varepsilon}^p$$
$$=s\,de^p$$

On the other hand, the use of effective stress-strain concept as given by Eqn. (26) for geomaterials is unreasonable as the volumetric plastic deformation of these materials can not be ignored. For geomaterials, the endochronic or the multi-response theory described below, which treat the volumetric and deviatoric deformations separately can be effectively used. In metal plasticity, the results of uniaxial tests are only used, and the following relation is introduced

$$\sigma_e=\sqrt{3J_2^\sigma}\,(=\sigma_{11})$$

Then the effective strain is usually written as

$$d\varepsilon_e^p=\sqrt{2\,d\boldsymbol{e}^p\cdot d\boldsymbol{e}^p/3}$$

This is merely written in this form in order to adjust coefficients in Eqn. (27).

4. 3. Multi-response theory under "weakly" cyclic loading

When the softening behaviour is not taken into account, elastic and plastic responses in multi-response theory are generally written in the following forms:

$$\sigma_i = \Phi_i^e(\varepsilon^e)$$
$$= \int_0^\infty \phi_i^e exp(-\varepsilon_j^e \xi_j) d\xi \tag{28}$$

$$\sigma_i = \Phi_i^p(\varepsilon^p)$$
$$= \int_0^\infty \phi_i^p exp(-\varepsilon_j^p \xi_j) d\xi \tag{29}$$

Note that the stress and strain are represented in the vector form.

$$(\sigma_i) = (\sigma_{xx},\ \sigma_{yy},\ \sigma_{zz},\ \sigma_{yz},\ \sigma_{zx},\ \sigma_{xy})^T$$
$$(\varepsilon_i) = (\varepsilon_{xx},\ \varepsilon_{yy},\ \varepsilon_{zz},\ \varepsilon_{yz},\ \varepsilon_{zx},\ \varepsilon_{xy})^T$$

In the following sections, the elasto-plastic multi-response theory will be described for hydrostaticaly symmetric materials keeping in mind the conventional triaxial tests.

4. 3. 1. Plastic response

The deviatoric and volumetric responses for hydrostatically symmetric materials can be written as:

$$s = \phi^p(e^p,\ \bar{\varepsilon}^p)$$
$$\bar{\sigma} = \psi^p(\bar{\varepsilon}^p,\ e^p) \tag{30}$$

When the plastic response is written as in Eqn. (30), the vectorial yield function is defined as:

$$f = \left\{ \begin{array}{l} f_1 \\ \\ f_2 \end{array} \right\} = o, \qquad \begin{array}{l} f_1 = s - \phi^p(e^p,\ \bar{\varepsilon}^p) \\ \\ f_2 = -\bar{\sigma} + \psi^p(\bar{\varepsilon}^p,\ e^p) \end{array}$$

Provided that plastic response does not involve the softening phenomenon, upper stress surface can be written in the following form by using Laplace transformations:

$$s = s_0 + \int_0^\infty \phi_1^p(\xi) \Lambda(\bar{\varepsilon}^p;\ \xi) d\xi + \int_0^\infty \phi_2^p(\eta) \Lambda(e^p;\ \eta) d\eta$$
$$+ \int_0^\infty \int_0^\infty \phi_3^p(\xi,\ \eta) \Lambda(\bar{\varepsilon}^p;\ \xi) d\xi \Lambda(e^p,\ \eta) d\eta$$

$$\bar{\sigma} = \bar{\sigma}_0 - \int_0^\infty \psi_1^p(\eta) \Lambda(e^p;\ \eta) d\eta + \int_0^\infty \psi_2^p(\xi) \Lambda(\bar{\varepsilon}^p;\ \xi) d\xi \tag{31}$$
$$+ \int_0^\infty \int_0^\infty \psi_3^p(\eta,\ \xi) \Lambda(e^p;\ \eta) d\eta \Lambda(\bar{\varepsilon}^p;\ \xi) d\xi$$

Where

$$\Lambda(a;\ \alpha)=1-exp(-a\alpha)$$

As a preparation for the asymptotic expansion of the response (31), the variables are replaced by $\tau=1/\eta$, $\omega=1/\xi$. Thus, we have

$$\begin{aligned} s=s_0+&\int_0^\infty \mu_1^p(\omega)\Gamma(\bar{\varepsilon}^p;\ \omega)d(\ln\omega)+\int_0^\infty \mu_2^p(\tau)\Gamma(e^p;\ \tau)d(\ln\tau)\\ &+\int_0^\infty\int_0^\infty \mu_3^p(\omega,\ \tau)\Gamma(\bar{\varepsilon}^p;\ \omega)d(\ln\omega)\Gamma(e^p;\ \tau)d(\ln\tau)\\ \bar{\sigma}=\bar{\sigma}_0-&\int_0^\infty \chi_1^p(\tau)\Gamma(e^p;\ \tau)d(\ln\tau)+\int_0^\infty \chi_2^p(\omega)\Gamma(\bar{\varepsilon}^p;\ \omega)d(\ln\omega)\\ &+\int_0^\infty\int_0^\infty \chi_3^p(\tau,\ \omega)\Gamma(e^p;\ \tau)d(\ln\tau)\Gamma(\bar{\varepsilon}^p;\ \omega)d(\ln\omega) \end{aligned} \tag{32}$$

Here

$$\mu_1^p(\omega)=\phi_1^p(1/\omega)/\omega,\ \mu_2^p(\tau)=\phi_2^p(1/\tau)/\tau,$$
$$\mu_3^p(\omega,\ \tau)=\phi_3^p(1/\omega,\ 1/\tau)/\omega\tau$$

and

$$\chi_1^p(\tau)=\psi_1^p(1/\tau)/\tau,\ \chi_2^p(\omega)=\psi_2^p(1/\omega)/\omega,$$
$$\chi_3^p(\tau,\ \omega)=\psi_3^p(1/\tau,\ 1/\omega)/\tau\omega$$

are called as the deviatoric and volumetric spectra respectively. And also

$$\Gamma(a;\beta)=1-exp(-a/\beta)=\Lambda(a;\ 1/\beta)$$

The incremental responses of plastic responses given by Eqn. (30) or (31) are written as follows:

$$\begin{Bmatrix} ds \\ d\bar{\sigma} \end{Bmatrix}=\begin{bmatrix} G_1^p & G_2^p \\ K_1^p & K_2^p \end{bmatrix}\begin{Bmatrix} de^p \\ d\bar{\varepsilon}^p \end{Bmatrix} \tag{33}$$

where

$$G_1^p=\partial\phi^p/\partial e^p,\qquad G_2^p=\partial\phi^p/\partial\bar{\varepsilon}^p,$$
$$K_1^p=\partial\psi^p/\partial\bar{\varepsilon}^p,\qquad K_2^p=\partial\psi^p/\partial e^p$$

or conversely

$$\begin{Bmatrix} de^p \\ d\bar{\varepsilon}^p \end{Bmatrix} = \begin{bmatrix} 1/h_s & \mu/h_s \\ \beta/h_v & 1/h_v \end{bmatrix} \begin{Bmatrix} ds \\ d\bar{\sigma} \end{Bmatrix} \tag{34}$$

where

$$h_s = G_1^p + \mu K_2^p, \qquad \mu = -G_2^p/K_1^p,$$
$$h_v = K_1^p + \beta G_2^p, \qquad \beta = -K_2^p/G_1^p$$

Here, h_s and h_v are the hardening parameters for shearing and volumetric variation respectively. μ is the internal friction coefficient and β is the dilatancy parameter.

If the direction of the plastic strain increment is assumed to be coaxial with the direction of stress, Eqn. (34) becomes

$$\begin{aligned} de^p &= \frac{1}{h_s}\boldsymbol{m}\otimes(\boldsymbol{m}+\mu\boldsymbol{n})d\sigma \\ d\bar{\varepsilon} &= \frac{1}{h_v}\boldsymbol{n}\otimes(\beta\boldsymbol{m}+\boldsymbol{n})d\sigma \end{aligned} \tag{35}$$

Where $\boldsymbol{m}$, $\boldsymbol{n}$ unit vectors defined by Eqn. (13). From these, the followings are obtained:

$$\begin{aligned} d\varepsilon^p &= de^p + d\bar{\varepsilon}^p = \boldsymbol{C}^p d\sigma \\ \boldsymbol{C}^p &= \frac{1}{h_s}\boldsymbol{m}\otimes(\boldsymbol{m}+\mu\boldsymbol{n}) + \frac{1}{h_v}\boldsymbol{n}\otimes(\beta\boldsymbol{m}+\boldsymbol{n}) \end{aligned} \tag{36}$$

Differentiating Eqn. (32), the plasticity spectra can be asymptotically written as

$$\mu_{23}^p(\tau;\ \bar{\varepsilon}^p) = \lim_{k\to\infty}\frac{(-1)^{k+1}}{(k-1)!}\tau^k\frac{\partial^k s}{\partial\tau^k}(k\tau,\ \bar{\varepsilon}^p) \tag{37}$$

$$\mu_{23}^p(\tau;\ \bar{\varepsilon}^p) = \mu_2^p(\tau) + \int_0^\infty \mu_3^p(\omega,\ \tau)\Gamma(\bar{\varepsilon}^p;\ \omega)d(\ln\omega)$$

$$\chi_{23}^p(\tau;\ e^p) = \lim_{k\to\infty}\frac{(-1)^{k+1}}{(k-1)!}\omega^k\frac{\partial^k\bar{\sigma}}{\partial\omega^k}(k\omega,\ e^p) \tag{38}$$

$$\chi_{23}^p(\omega;\ e^p) = \chi_2^p(\omega) + \int_0^\infty \chi_3^p(\tau,\ \omega)\Gamma(e^p;\ \tau)d(\ln\tau)$$

Accordingly, when responses are approximately determined, we have

$$s = s_0 + \sum_i a_{1i}\Gamma(\bar{\varepsilon}^p;\ \omega_i) + a_{2i}\Gamma(e^p;\ \tau_i) + a_{3ii}\Gamma(\bar{\varepsilon}^p;\ \omega_i)\Gamma(e^p;\ \tau_i) \tag{39}$$

$$a_{1i} = \mu_1^p(\omega_i)\Delta\omega_i/\omega_i,\ \ a_{2i} = \mu_2^p(\tau_i)\Delta\tau_i/\tau_i,$$

$$a_{3ii}=\mu_3^p(\omega_i,\ \tau_i)\Delta\omega_1\Delta\tau_i/\omega_i\tau_i$$

$$\bar{\sigma}=\bar{\sigma}_0-\sum_i\{b_{1i}\Gamma(e^p;\ \tau_i)-b_{2i}\Gamma(\bar{\varepsilon}^p;\ \omega_i)-b_{3ii}\Gamma(e^p;\ \tau_i)\Gamma(\bar{\varepsilon}^p;\ \omega_i)\} \tag{40}$$

$$b_{1i}=\chi_1^p(\tau_i)\Delta\tau_i/\tau_i,\ b_{2i}=\chi_2^p(\omega_i)\Delta\omega_i/\omega_i,$$

$$b_{3ii}=\chi_3^p(\tau_i,\ \omega_i)\Delta\tau_i\Delta\omega_i/\tau_i\omega_i$$

Discretized spectral points $(\tau_i,\ \omega_i)$

$$\mu_{23}(e^p;\ \bar{\varepsilon}^p=const)=e^p\frac{\partial s}{\partial e^p}(e^p,\ \bar{\varepsilon}^p=const)$$

$$\chi_{23}(\bar{\varepsilon}^p;\ e^p=const)=\bar{\varepsilon}^p\frac{\partial\bar{\sigma}}{\partial\bar{\varepsilon}^p}(\bar{\varepsilon}^p;\ e^p=const)$$

are determined from the curves of the above expressions obtained from triaxial tests. Once discretized spectral points τ_i, ω_i are obtained, coefficients a_{1i}, a_{2i}, a_{3ii}; b_{1i}, b_{2i}, b_{3ii} of response functions (39) and (40) can be easily determined from experimental data by the least square method.

4. 3. 2. Elastic Response

In almost all rocks, plastic strains are observed from the very beginning of the application of load and the response of elastic component is also non-linear. As the elastic response can be written in the same form as that for the plastic response, we herein present only the resulting expressions:

Response functions

$$\begin{aligned}s&=\phi^e(e^e,\ \bar{\varepsilon}^e)\\&=s_0+\int_0^\infty\phi_1^e(\xi)\Lambda(\bar{\varepsilon}^e;\ \xi)d\xi+\int_0^\infty\phi_2^e(\eta)\Lambda(e^e;\ \eta)d\eta\\&\quad+\int_0^\infty\int_0^\infty\phi_3^e(\xi,\ \eta)\Lambda(\bar{\varepsilon}^e;\ \xi)d\xi\Lambda(e^e,\ \eta)d\eta\\&=s_0+\int_0^\infty\mu_1^e(\omega)\Gamma(\bar{\varepsilon}^e;\ \omega)d(\ln\omega)+\int_0^\infty\mu_2^e(\tau)\Gamma(e^e;\ \tau)d(\ln\tau)\\&\quad+\int_0^\infty\int_0^\infty\mu_3^e(\omega,\ \tau)\Gamma(\bar{\varepsilon}^e;\ \omega)d(\ln\omega)\Gamma(e^e,\ \tau)d(\ln\tau)\end{aligned}\tag{41}$$

$\mu_1^e(\omega)$, $\mu_2^e(\tau)$, $\mu_3^e(\omega,\ \tau)$: deviatoric spectra

$$\begin{aligned}\bar{\sigma}&=\psi^e(\bar{\varepsilon}^e,\ e^e)\\&=\bar{\sigma}_0+\int_0^\infty\psi_1^e(\eta)\Lambda(e^e;\ \eta)d\eta+\int_0^\infty\psi_2^e(\xi)\Lambda(\bar{\varepsilon}^e;\ \xi)d\xi\\&\quad+\int_0^\infty\int_0^\infty\psi_3^e(\eta,\ \xi)\Lambda(e^e,\ \eta)d\eta\Lambda(\bar{\varepsilon}^e;\ \xi)d\xi\end{aligned}$$

$$= \bar{\sigma}_0 + \int_0^\infty \chi_1^e(\tau)\Gamma(e^e;\ \tau)d(\ln\tau) + \int_0^\infty \chi_2^e(\omega)\Gamma(\bar{\varepsilon}^e;\ \omega)d(\ln\omega)$$
$$+ \int_0^\infty \int_0^\infty \chi_3^e(\tau,\ \omega)\Gamma(e^e;\ \tau)d(\ln\tau)\Gamma(\bar{\varepsilon}^e;\ \omega)d(\ln\omega) \qquad (42)$$

$\chi_1^e(\tau)$, $\chi_2^e(\omega)$, $\chi_3^e(\tau,\ \omega)$: volumetric spectra

Incremental responses

$$\begin{Bmatrix} ds \\ d\bar{\sigma} \end{Bmatrix} = \begin{bmatrix} G_1^e & G_2^e \\ K_1^e & K_2^e \end{bmatrix} \begin{Bmatrix} de^e \\ d\bar{\varepsilon}^e \end{Bmatrix}$$

$$G_1^e = \partial\phi^e / \partial e^e, \qquad G_2^e = \partial\phi^e / \partial\bar{\varepsilon}^e,$$
$$K_1^e = \partial\psi^e / \partial e^e, \qquad K_2^e = \partial\psi^e / \partial\bar{\varepsilon}^e$$

or

$$\begin{Bmatrix} de^e \\ d\bar{\varepsilon}^e \end{Bmatrix} = \begin{bmatrix} 1/g_s & \lambda/g_s \\ \alpha/g_v & 1/g_v \end{bmatrix} \begin{Bmatrix} ds \\ d\bar{\sigma} \end{Bmatrix}$$

$$g_v = K_1^e + \alpha G_2^e, \qquad \alpha = -K_2^e / G_2^e,$$
$$g_s = G_1^e + \lambda K_2^e, \qquad \lambda = -G_2^e / K_2^e$$

As the direction of elastic strain coincide with the direction of incremental stress, we can write the followings

$$d\boldsymbol{e}^e = \frac{1}{g_s}\boldsymbol{m}^* \otimes (\boldsymbol{m} + \lambda \boldsymbol{n})\, d\bar{\sigma}$$
$$d\bar{\boldsymbol{\varepsilon}}^e = \frac{1}{g_v}\boldsymbol{n}^* \otimes (\alpha \boldsymbol{m} + \boldsymbol{n})\, d\bar{\sigma}$$

However, note that we used the following identities in the above expressions:

$$\boldsymbol{m}^* = \frac{d\boldsymbol{s}}{||d\boldsymbol{s}||} = \boldsymbol{m}^{-1}, \quad \boldsymbol{n}^* = \frac{d\bar{\sigma}}{||d\bar{\sigma}||}\boldsymbol{n}^{-1}$$

As the asymtotic expansion of elastic spectra and the determination of its discretized form are similar to those of the plastic response, they will not be presented herein.

4. 4. Non-associated flow theory with a dilatancy function

In this section, the Drucker-Prager model of isotropic strain hardening type is considered:

$$f(\sigma,\ \varkappa)=\alpha\bar{\sigma}+s-K(e^p,\ \bar{\varepsilon}^p)=0 \tag{43}$$

$$\alpha=\text{constant}$$

This model is hydrostatically symmetric with respect to stress and strain. More concretely, $(s,\ \bar{\sigma})$ and $(e^p,\ \bar{\varepsilon}^p)$ are introduced and Lode angle is not considered. Then the base vectors defined in Eqn. (13) are:

$$\boldsymbol{m}=\frac{\partial s}{\partial \boldsymbol{s}}=\frac{\boldsymbol{s}}{s}=\frac{d\boldsymbol{e}^p}{||d\boldsymbol{e}^p||},\quad \boldsymbol{n}=\frac{\partial\bar{\sigma}}{\partial\bar{\sigma}}=\frac{\bar{\sigma}}{\bar{\sigma}}=\frac{d\bar{\varepsilon}^p}{||d\bar{\varepsilon}^p||} \tag{44}$$

$$\frac{\partial\theta^{\sigma}}{\partial\sigma}=0,\quad \frac{\partial\theta^{\varepsilon,p}}{\partial\varepsilon^p}=0$$

($\theta^{\varepsilon,p}$:Lode angle associated with plastic strain ε^p).

When the plastic strain and its increment depend upon the Lode angle, note the following:

$$\frac{d\boldsymbol{e}^p}{||d\boldsymbol{e}^p||}\neq\frac{\boldsymbol{e}^p}{||\boldsymbol{e}^p||}$$

Let us define a dilatancy function as follows:

$$\beta=\frac{d\bar{\varepsilon}^p}{||d\boldsymbol{e}^p||} \tag{45}$$

where

$$d\bar{\varepsilon}^p=d(tr(\boldsymbol{\varepsilon}^p)/\sqrt{3})=tr(d\boldsymbol{\varepsilon}^p)/\sqrt{3}$$

$$||d\boldsymbol{e}^p||=(de^p_{ij}de^p_{ij})^{1/2}$$

However, it should be noted that as the hydrostatically symmetric concept is introduced, the increment de^p of e^p coincides with $||d\boldsymbol{e}^p||$:

$$de^p=||d\boldsymbol{e}^p||$$

In addition, as the direction of the incremental plastic strain coincides with that of the total stress, the flow law (12) becomes:

$$d\boldsymbol{e}^p=\lambda\frac{\partial g}{\partial s}\boldsymbol{m},\quad d\bar{\varepsilon}^p=\lambda\frac{\partial g}{\partial\bar{\sigma}}\boldsymbol{n}$$

Accordingly, we have

$$\beta=\frac{d\bar{\varepsilon}^p}{de^p}=\frac{\partial g}{\partial\bar{\sigma}}\Big/\frac{\partial g}{\partial s} \tag{46}$$

By using the dilatancy function, one gets

$$\frac{\partial g}{\partial \sigma}=\frac{\partial g}{\partial s}(\boldsymbol{m}+\alpha \boldsymbol{n})$$

and derivating the yield function (23) yields

$$\frac{\partial f}{\partial \sigma}=\boldsymbol{m}+\alpha \boldsymbol{n}$$

Subsituting the above expressions in the constitutive equation (23) results in

$$d\sigma=\boldsymbol{D}^{ep}d\varepsilon \tag{47}$$

$$\boldsymbol{D}^{ep}=\boldsymbol{D}^{e}-\boldsymbol{D}^{e}(\boldsymbol{m}+\beta \boldsymbol{n})\otimes \boldsymbol{D}^{e}(\boldsymbol{m}+\alpha \boldsymbol{n})$$

The hardening parameter h' in the second equation of the equations (16) is obtained as:

$$\begin{aligned} h' &= h/\frac{\partial g}{\partial s} \\ &= (\frac{\partial K}{\partial e^p}\boldsymbol{m}+\frac{\partial K}{\partial \bar{\varepsilon}^p}\boldsymbol{n})\cdot(\boldsymbol{m}+\beta \boldsymbol{n}) \\ &= \frac{\partial K}{\partial e^p}+\beta\frac{\partial K}{\partial \bar{\varepsilon}^p} \end{aligned} \tag{48}$$

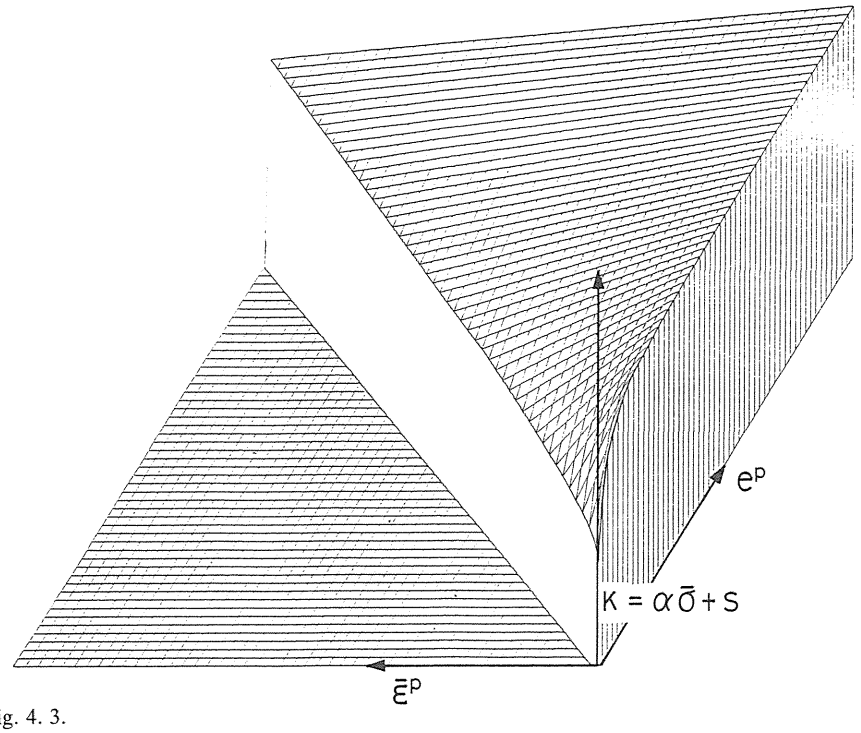

Fig. 4. 3.

4. 4. 1. Hardening spectra and Dilatancy spectra

Next, how to express the hardening function $K(e^p, \bar{\varepsilon}^p)$ will be considered. From the experimental data of triaxial tests on geomaterials, a set of curves of the hardening parameter as a linear sum of stresses and the deviatoric strain e^p can be drawn as shown in Fig. 5. 2 by taking the volumetric strain as a parameter ε^p. However, it should be noted that the softening is omitted in this representation as it is a structural property depending on the testing method. When this set of curves are redrawn on the surface of $(e^p, \bar{\varepsilon}^p)$, a surface shown in Fig. 4. 3 is obtained. In Fig. 4. 3, the surface is monotonically increasing with respect to e^p for ε^p=constant and monotonically decreasing with respect to ε^p for e^p constant. Using the Laplace transformations, one has

$$K(e^p, \bar{\varepsilon}^p)=K_0+\int_0^\infty\int_0^\infty \phi(\xi, \eta)\Lambda_i(e^p; \xi)\Lambda_d(\bar{\varepsilon}^p, \eta)d\xi d\eta \tag{49}$$

where

$$\Lambda_i(e^p; \xi)=1-exp(-e^p\xi)$$

$$\Lambda_d(\bar{\varepsilon}^p; \eta)=exp(-\bar{\varepsilon}^p\eta)$$

The above expression is rewritten as a preparation for the discretized approximation:

$$K(e^p, \bar{\varepsilon}^p)=K_0=\int_0^\infty\int_0^\infty \mu(\tau, \omega)\Gamma_i(e^p; \tau)\Gamma_d(\bar{\varepsilon}^p, \omega)d(\ln\tau)d(\ln\omega) \tag{50}$$

where

$$\mu(\tau, \omega)=\phi(1/\tau, 1/\tau)/\tau\omega \tag{51}$$

$$\Gamma_i(e^p, \tau)=1-exp(-e^p/\tau)=\Lambda(e^p; 1/\tau)$$

$$\Gamma_d(e^p, \tau)=exp(-\bar{\varepsilon}^p\omega)=\Lambda(\bar{\varepsilon}^p; 1/\omega) \tag{52}$$

$\mu(\tau, \omega)$ is called hardening spectra. Dilatancy function β is represented in the following form as in terms of volumetric stress $\bar{\sigma}$ as the dilatancy decreases with the increase in compressive stresses:

$$\beta(\bar{\sigma})=\int_0^\infty \psi(\xi)\Lambda_d(\bar{\sigma}; \xi)d\xi \tag{53}$$

or

$$\beta(\bar{\sigma})=\int_0^\infty \lambda(\tau)\Gamma_d(\bar{\sigma}; \tau)d(\ln\tau) \tag{54}$$

Note that the tensile stress is taken as positive. The following expression is called the dilatancy spectra.

$$\lambda(\tau)=\psi(1/\tau)/\tau \tag{55}$$

4. 4. 2. The asypmtotic expansions of hardening and dilatancy functions and their discretized approximations

Differentiating $K(e^p, \bar{\varepsilon}^p)$ with respect to e^p k times, and replacing $\xi\exp(-e^p\xi)$ by δ function yields:

$$\frac{\partial^k K}{\partial(e^p)^k}=(-1)^{k+1}\int_0^\infty \phi_{ep}(\xi;\ \bar{\varepsilon}^p)\xi^k exp(-e^p\xi)d\xi \tag{56}$$

$$=\lim_{k\to\infty}(-1)^{k+1}\frac{k!}{(e^p)^{k+1}}\phi_{ep}(k/e^p;\ \bar{\varepsilon}^p)$$

Note that we used the following.

$$\phi_{ep}(\xi;\ \bar{\varepsilon}^p)=\int_0^\infty \phi(\xi,\ \eta)\Lambda_d(\varepsilon^p;\ \eta)d\eta$$

Eqn. (56) means the following

$$\phi_{ep}(\xi;\ \bar{\varepsilon}^p)=\lim_{k\to\infty}\frac{(-1)^{k+1}}{k!}(\frac{k}{\xi})^{k+1}\frac{\partial^k K(k/\xi,\ \varepsilon^p)}{\partial(k/\xi)^k}$$

Through variable changes $\tau=1/\xi$, the following is obtained:

$$\mu_{ep}(\tau;\ \bar{\varepsilon}^p)=\lim_{k\to\infty}\frac{(-1)^{k+1}}{(k-1)!}(k\tau)^k\frac{\partial^k K(k\tau,\ \bar{\varepsilon}^p)}{\partial(k\tau)^k} \tag{57}$$

where

$$\mu_{ep}(\tau;\ \bar{\varepsilon}^p)=\int_0^\infty \mu(\tau;\ \omega)\Gamma_d(\bar{\varepsilon}^p;\ \omega)d(\ln\omega)$$

In a similar manner, the dilatancy function is asymptotically expanded in the following form:

$$\psi(\xi)=\lim_{k\to\infty}\frac{(-1)^k}{k!}(\frac{k^{k+1}}{\xi})\frac{d^k\beta(k/\xi)}{d(k/\xi)}$$

or

$$\lambda(\tau)=\lim_{k\to\infty}\frac{(-1)^k}{(k-1)}(k\tau)^k\frac{d^k\beta(k\tau)}{d(k\tau)^k}$$

As a first approximation to the asymptotic equation (57), we specify the following:

$$\mu_{ep}(\tau;\ \bar{\varepsilon}^p)\,|_{k=1}=\tau\frac{\partial K(\tau,\ \bar{\varepsilon}^p)}{\partial\tau}$$

We obtain the curves of the following expression for each constant $\bar{\varepsilon}^p$ from the experimental data as shown in Fig. 4. 4:

$$\mu_{ep}(e^p;\ \bar{\varepsilon}^p=const.)=e^p\frac{\partial K(e^p,\ \bar{\varepsilon}^p=const.)}{\partial e^p} \tag{58}$$

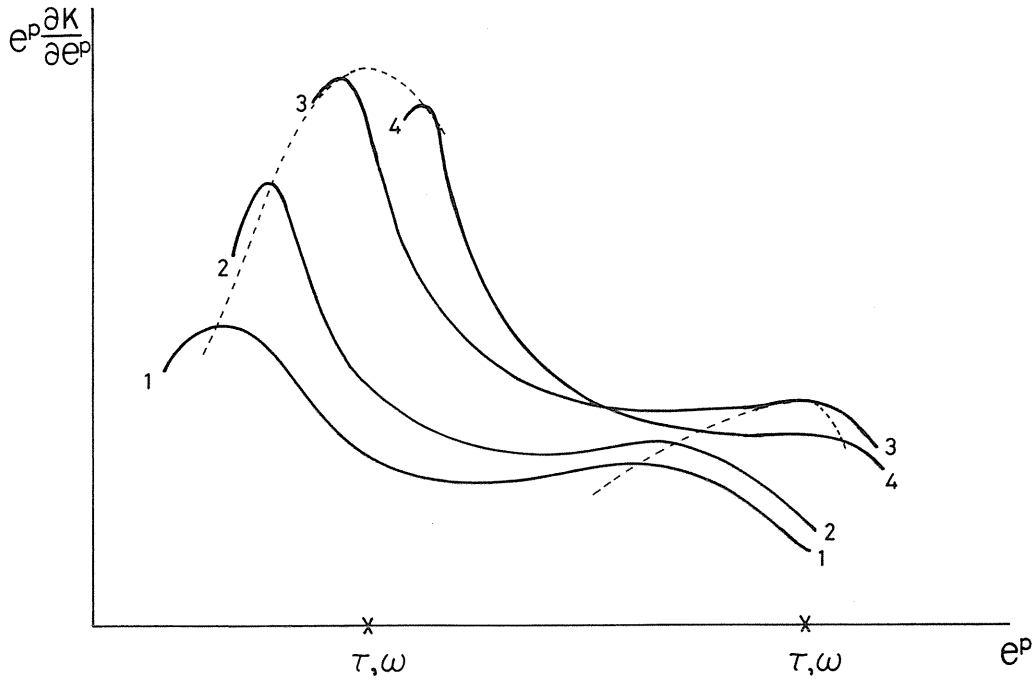

Fig. 4. 4.

From the peak points of these curves in Fig. 4. 4, spectra points (τ_1, ω_1), (τ_2, ω_2), (τ_3, ω_3), ... are determined. With the spectra points (τ_k, ω_k), k=1, 2, ... the hardening function is represented in the following form.

$$K=K_0+\sum_k a_k \Gamma_i(e^p;\ \tau_k)\Gamma_d(\bar{\varepsilon}^p;\ \omega_k) \tag{59}$$

However, it should be noted that, to select the peak points only, the surface integration of Eqn. (49) is represented in the diagonalized form. Additionally,

$$a_k=\lambda(\tau_k,\ \omega k)\Delta\tau_k\Delta\omega_k/\tau_k\omega_k$$

The coefficient a_k is determined from the experimental data by using the least square method. More explicitly, the error function is defined as

$$E=\frac{1}{2}[K-\{K_0+\sum_k \Gamma_i(e^p;\tau_k)\Lambda_d(\bar{\varepsilon}^p;\ \omega_k)\}]^2 \tag{60}$$

and the coefficient a_k is determined from the following linear equation system:

$$\frac{\partial E}{\partial a_k}=0,\ k=1,\ 2,\ \ldots \tag{61}$$

The discretized form of the dilatancy function β is also obtained from the same procedure. As a first approximation to $\lambda(\tau)$, the following is specified

$$\lambda(\tau)|_{k=1}=-\tau\frac{\partial\beta}{\partial\tau}$$

and discretized spectra points τ_m: m=1, 2, ... are determined from the graphs of experimental data

$$\lambda(\bar{\sigma})=-\bar{\sigma}\frac{\partial\beta}{\partial\bar{\sigma}} \tag{62}$$

and the discretized form of the dilatancy function β is represented in the following form:

$$\beta=\sum_m b_m\Gamma_d(\bar{\sigma};\ \tau_m) \tag{63}$$
$$b_m=\lambda(\tau_m)\Delta\tau_m/\tau_m$$

Coefficient b_m is obtained from the minimization of the error function:

$$E=\frac{1}{2}[\beta-\sum_m b_m\Gamma_d(\bar{\sigma};\ \tau_m)]^2 \tag{64}$$

$$\frac{\partial E}{\partial b_m}=0,\ k=1,\ 2,\ \ldots \tag{65}$$

4. 5. Data processing and determination of response functions

The physical properties of geomaterials are usually determined from triaxial tests in laboratory. In this section, the data processing system and determination of response functions from the experimental data will be described.

Since the experimental data has a scattering, it is difficult to directly derivate Eqns. (58) and (62). Therefore, the smooting procedure is performed and spectra points are determined. Now, let us assume that, at descretized points X_i, i=1,2,...,N $f_i=f(X_i)$ are observed and let us define the dot product of functions $g(X)$ and $h(X)$ as

$$<g,h>=\sum_{i=1}^{N} g(x_i)h(x_i)=\sum_{i=1}^{N} g_ih_i$$

Taking $a=minX_i$, $b=maxX_i$, a set of orthogonal polynominals on the space $[a,b]$ is

obtained by the recurrence equation

$$P_{i+1}(x)=A_i(x-B_i)P_i(x)-C_iP_{i-1}(x),\quad i=1,2,3,\ldots \tag{66}$$

where

A_i : nonzero constant

$$B_i=\frac{<xP_i,P_i>}{<P_i,P_i>}\quad C_i=\frac{A_i<P_i,P_i>}{A_{i-1}<P_{i-1},P_{i-1}>}$$

and we set $P_{-1}=0$, $P_0=\alpha_0$(constant).

To fit the observed data by an k-th order polynomial p(x), the error function is defined as

$$E=\sum_{i=1}^{N}\{f_i-p(x_i)\}^2$$

Using the orthogonal polynomials $\{P_i\}$, $p(x_i)$ can be represented as

$$p(x_i)=\sum_{j=1}^{k}d_jP_j(x_i)$$

the error E can be minimized in terms of d_j, then we have

$$\partial E/\partial d_i=-2\sum_{j=1}^{k}\{f_i-p(x_j)\}P_i(x_j)=0$$

from which, coefficients are obtained as

$$d_i=\frac{\sum_{i=1}^{N}f_iP_i(x_j)}{\sum_{i=1}^{N}\{P_i(x_j)\}^2},\quad i=0,1,2,\ldots$$

Note that the order k is kept to a minimum in order not to include the scattering of the experimental data.

5. Applications to Several Rocks

We have performed monotonic and "weak" cyclic triaxial tests on many rocks to specify the deformation behaviours of geomaterials. In this section, we show, first, the plastic deformation characteristics obtained from these tests. Then, we specify the parameters of the constitutive laws proposed in the previous section for the plastic response of Oya-tuff under monotone loading, and the elastic-plastic responses of Funyu-tuff and granite under cyclic loading, respectively. To verify the validity of the plastic response model for Oya-tuff, a triaxial test under monotone loading at several confining pressures is simulated by a finite element analysis.

5. 1. *Plastic response of Oya-tuff*

5. 1. 1. *Yield function*

Firstly, we start with the determination of the yielding function defined in Section 4.2.4. The initial and the peak yielding curves are plotted in the mean stress $\bar{\sigma}$ and deviatoric stress s space for several confining pressures in Fig. 5.1. The initial yielding point is defined as the point at which a volumetric non-linearity starts as seen in Fig. 5.1(a), and the peak yielding point is defined as the point at which peak strength is achieved as seen in Fig. 5.1(b). Both curves can be approximated by a straight line in $\bar{\sigma}$, s space, and it seems the peak yielding curve remains to be parallel to the initial yielding curve. It implies that the material can be assumed to be isotropic hardening, and the Drucker-Prager's yield function is adopted as the yield criterion:

$$f=\alpha\bar{\sigma}+s-K=0 \tag{67}$$

where, α is a constant, and K represents a hardening function. Then, α and the initial value of the hardening function, K_0 are obtained from Fig.5.1 for the initial yielding state as:

$$\alpha=-0.29,\quad K_0=5.8MN/m^2$$

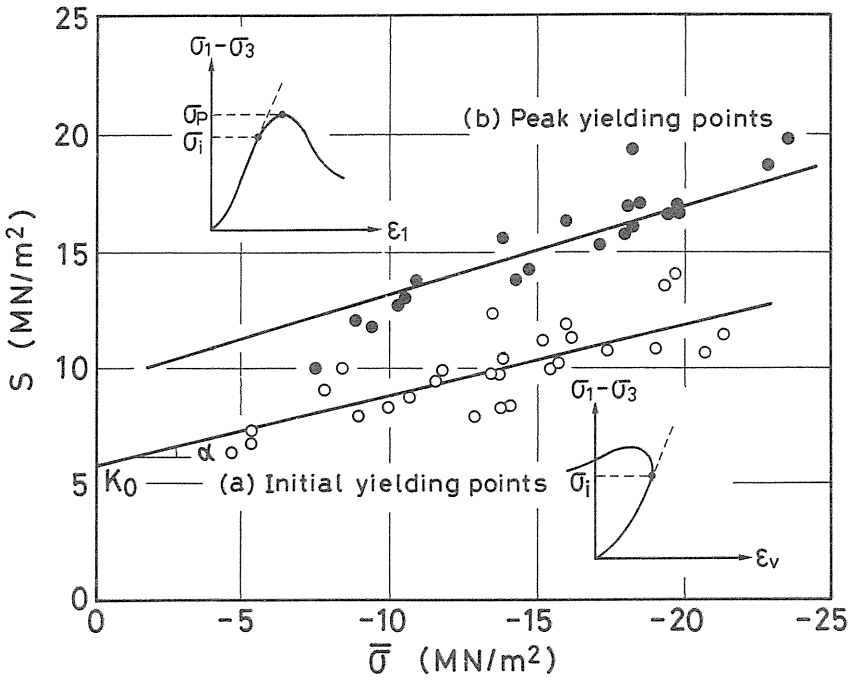

Fig. 5. 1. Initial and peak yielding conditions

5. 1. 2. *Hardening function*

Since the yielding function is represented by Eqn. (67), the hardening function can be described as

$$K=\alpha\bar{\sigma}+s. \tag{68}$$

The hardening behaviours of the deviatoric plastic strain, $K(e^p,\ \bar{\varepsilon}^p=const.)$, observed in experiments are shown by dashed lines in Fig. 5.2 for several levels of volumetric plastic strain, $\bar{\varepsilon}^p$. The hardening response is chosen as a monotonicaly increasing function for $\bar{\varepsilon}^p=const.$ in Fig. 5.2. These response curves can be approximated by low order orthogonal polynomials in this case. Then, by differentiating these curves and by calculating $(e^p\partial K/\partial e^p)_{\bar{\varepsilon}=const.}$, and plotting them (Fig. 5.3), we get two spectral points as:

$$\tau_1=7.1\times10^{-4},\ \tau_2=1.8\times10^{-3}\ \text{for}\ e^p$$

and

$$\omega_1=6.6\times10^{-5},\ \omega_2=2.0\times10^{-4}\ \text{for}\ \bar{\varepsilon}^p.$$

Then, the hardening response function is determined as

$$K=K_0+a_1\Gamma(e^p;\tau_1)\Gamma(\bar{\varepsilon}^p;\omega_1)+a_2\Gamma(e^p;\tau_2)\Gamma(\bar{\varepsilon}^p;\omega_2). \tag{69}$$

The initial value K_0 is determined from the initial yield surface in (Fig. 5.1(a)), and the values a_1 and a_2 are obtained by the least square method:

$$a_1=-2.1\ \text{MPa},\ a_2=18.9\ \text{MPa}.$$

The predicted curves using these values are shown by solid lines in Fig. 5.2.

5. 1. 3. Dilatancy function

The experimental results of Oya-tuff under monotone loading shows a dilatant behaviour at low confining pressures. Dilation takes place in association with shearing deformation under compressive loading. We show now, the relation between the volumetric strain $\bar{\varepsilon}^p$ and the integrated norms $\int\|de^p\|$ for various confining pressures in Fig. 5.4(a), and the corresponding the mean stress, $\bar{\sigma}$ in Fig. 5.4(b). Using the similar procedures for the hardening response function, we get the dilatancy function β as follows: These curves (Fig. 5.4) are approximated by polynomials of low order, and differentiating $\bar{\varepsilon}^p$ with respect to $\int\|de^p\|$, and plotting them against $\bar{\sigma}$. Then, we have the relation between the dilatancy factor and the mean stress, $\bar{\sigma}$ as shown in Fig. 5.5. Again, these points in Fig. 5.5 are approximated by low order orthogonal polynomials, and differentiating them, we get a spectral curve $-\bar{\sigma}d\beta/d\bar{\sigma}$ to $\bar{\sigma}$ (Fig. 5.6). We have two spectral points for dilatancy function β as

$$\tau_1=9.4\ \text{MPa},\ \tau_2=-16.1\ \text{MPa}.$$

The corresponding coefficients of the polynomial are obtained by the least square method:

$$a_1=-2.787,\ a_2=-1.175.$$

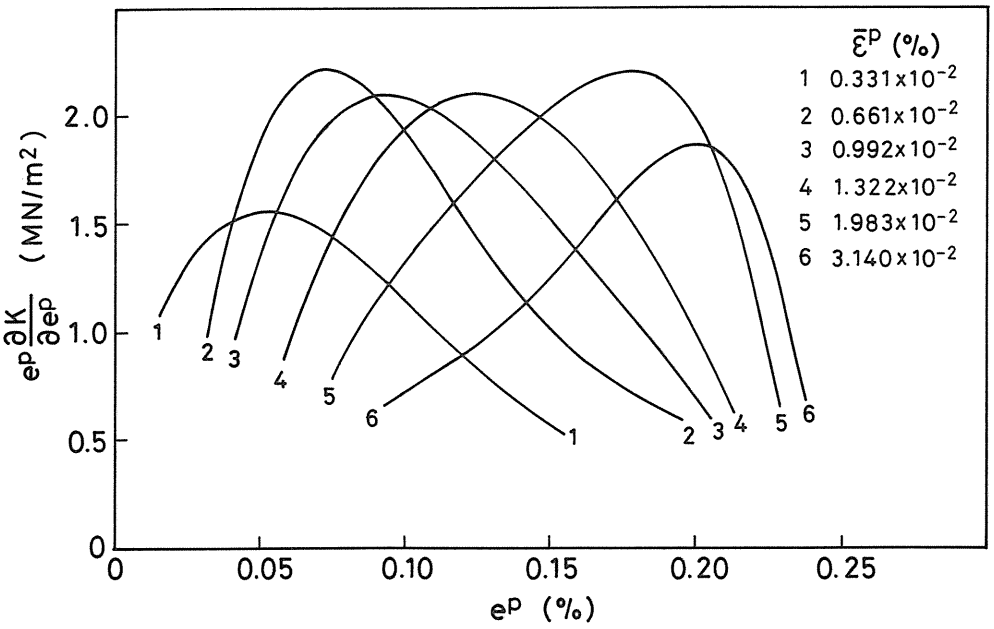

Fig. 5. 2. Hardening response (Oya-tuff)

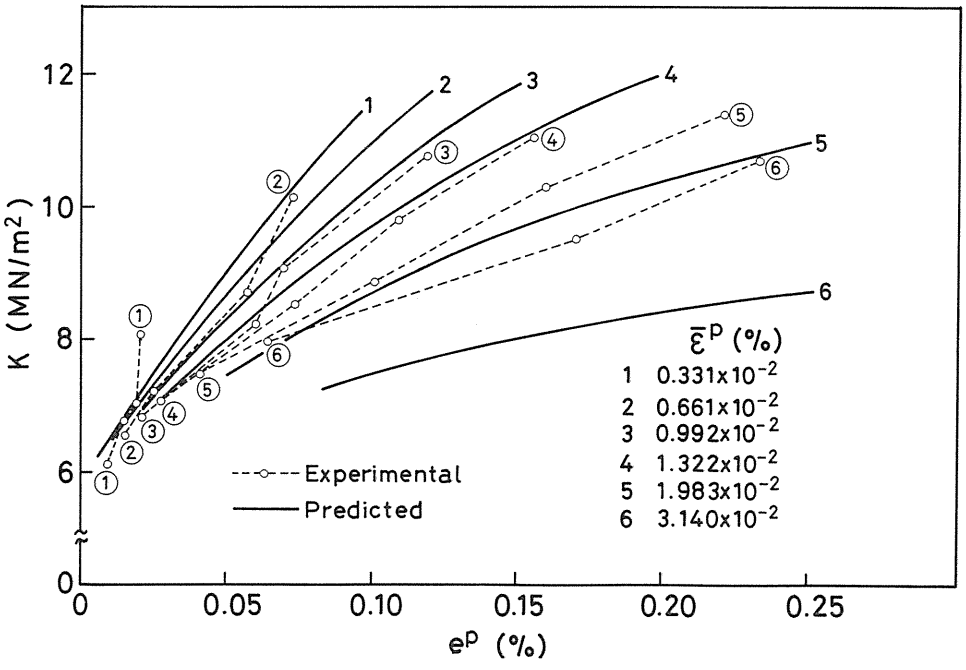

Fig. 5. 3. Hardening spectra

The dilatancy function obtained is shown by solid line in Fig. 5.7.

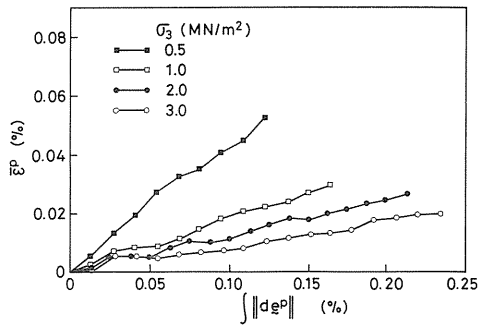

Fig. 5. 4a Volumetric plastic strain-deviatoric strain curves for various confining pressures (Oya-tuff)

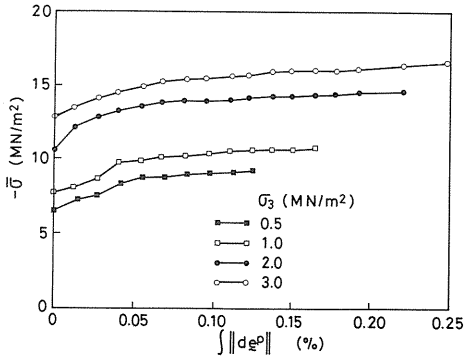

Fig. 5. 4b Volumetric stress-deviatoric strain curves for various confining pressures (Oya-tuff)

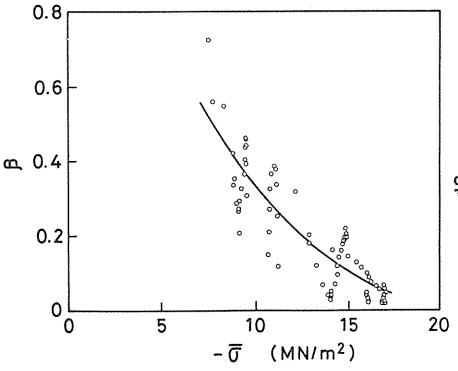

Fig. 5. 5. Dilatancy function (Oya-tuff)

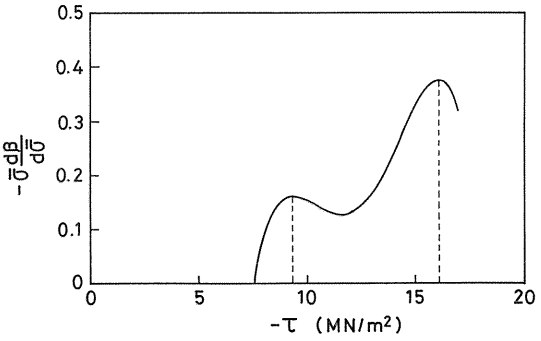

Fig. 5. 6. Dilatancy spectra (Oya-tuff)

5. 1. 4. *Numerical example*

Using the specified parameters of the constitutive equation for Oya-tuff, we simulate a triaxial test of Oya-tuff by the axisymmetric finite element analysis. The finite element mesh and the boundary conditions of the triaxial test are shown in Fig. 5.7. The lateral nodal forces which are equivalent to the confining pressure, and an equivalent axial incremental forced displacement were applied. Numerical results of the axial strain $\bar{\varepsilon}_1$ and the volumetric strain $\bar{\varepsilon}_v$ versus the differential stress $(\sigma_1-\sigma_3)$ are shown in Fig. 5.8 for two confining pressures, and are compared with experimental measurements. It is found that there is a good agreement between experimental and predicted responses.

5. 2. *Elastic and plastic of Funyu-tuff*

5. 2. 1. *Plastic response*

As explained in the previous section, in the multi-response theory, the plastic and

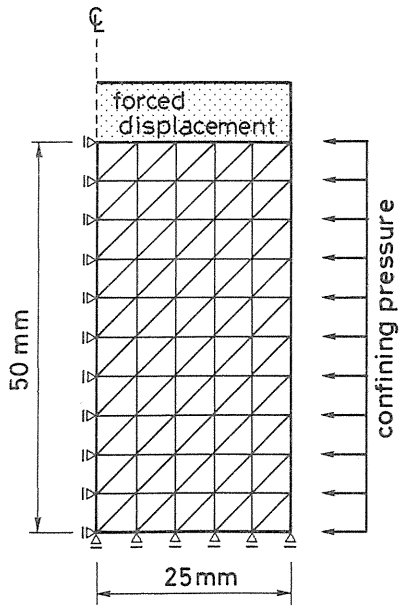

Fig. 5. 7. Finite element mesh and boundary conditions

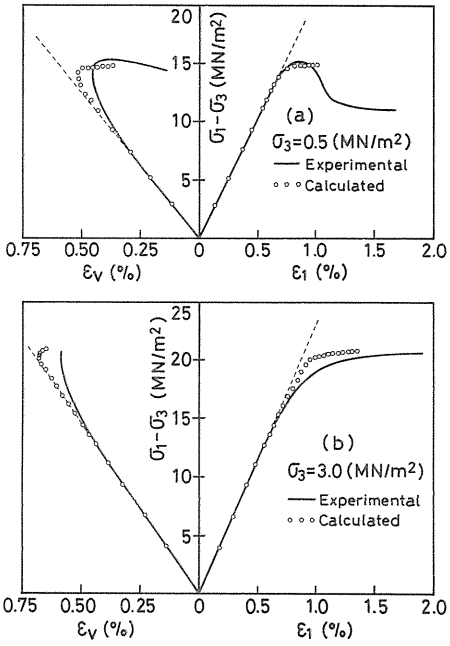

Fig. 5. 8. Comparison of predicted and measured differential stress-axial strain and volumetric strain curves

elastic strain responses are separated, and the material is treated hydrostatically symmetric, provided that its response is of isotropically hardening type, and deviatoric and volumetric responses are separated and on the basis of which, the incremental constitutive equation of a material is determined. As the material shows elasto-plastic behaviour from the very beginning of loading, there is a need to obtain the elastic and plastic strain responses separately. Therefore, we start to separate these responses during the initial hydrostatical loading also and carry out a series of cyclic loading in this stage. The stress paths for each tests are shown in Fig. 5.9. Typical curves of axial stress-axial strain and axial stress-lateral strain obtained during hydrostatic loading Fig. 5.10 and 5.11.

Figs. 5.12 to 5.16 show the plastic responses for $(\bar{\sigma}-\bar{\varepsilon}^p)$, $(\bar{\sigma}-\bar{e}^p)$, $(s-\bar{\varepsilon}^p)$, $(s-\bar{e}^p)$ and $(e^p-\bar{\varepsilon}^p)$. Figs. 5.17 to 5.21 show the determined response function for $s(e^p, \bar{\varepsilon}^p)$ and $\bar{\sigma}(e^p-\bar{\varepsilon}^p)$. From these data, deviatoric stress s and volumetric stress $\bar{\sigma}$ given in Eqn. (30) are determined. As decribed in the previous section, following the smoothing procedure and the polynomial approximation, the calculated spectra of the plastic response functions are shown in Figs. 5.22 and 5.23. From Fig. 5.24, the values of deviatoric plastic response spectra points are:

$$\omega_{11}=0.00140,\ \tau_{11}=0.0020$$

$$\omega_{12}=0.00203,\ \tau_{12}=0.0050$$

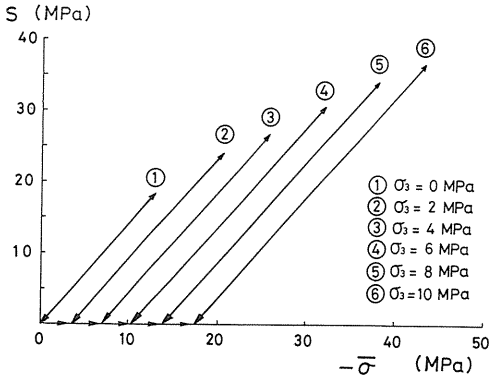

Fig. 5. 9. Stress paths

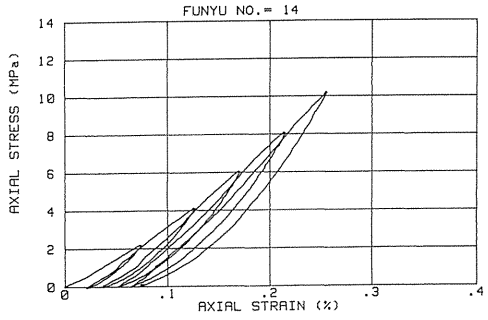

Fig. 5. 10. Axial stress-axial curves of Funyu-tuff in a cyclic test

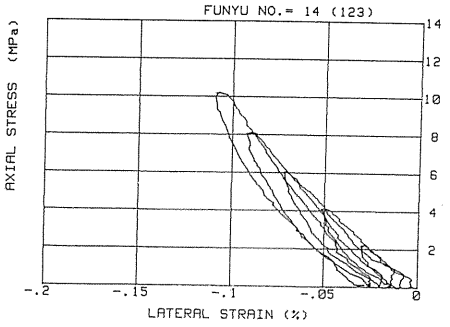

Fig. 5. 11. Axial stress-lateral strain curves of Funyu-tuff in a cyclic test

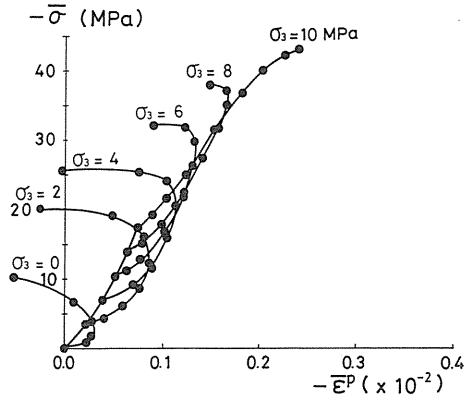

Fig. 5. 12. Volumetric stress-volumetric plastic strain curved of Funyu-tuff for various confining pressures

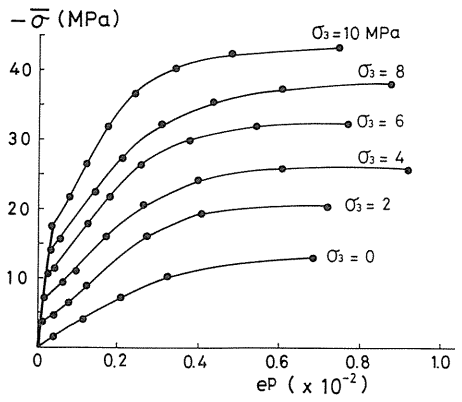

Fig. 5. 13. Volumetric stress-deviatoric plastic strain curves of Funyu-tuff for various confining pressures

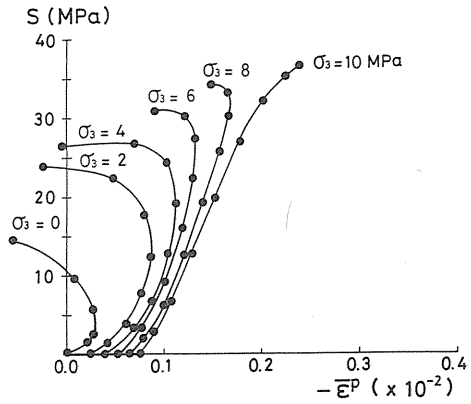

Fig. 5. 14. Deviatoric stress-volumetric plastic strain curves of Funyu-tuff for various confining pressure

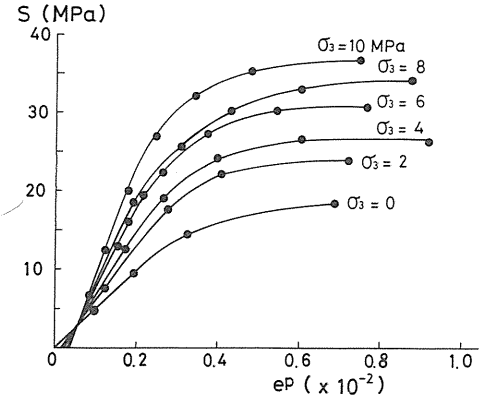

Fig. 5. 15. Deviatoric stress-deviatoric plastic strain curved of Funyu-tuff for various confining pressures

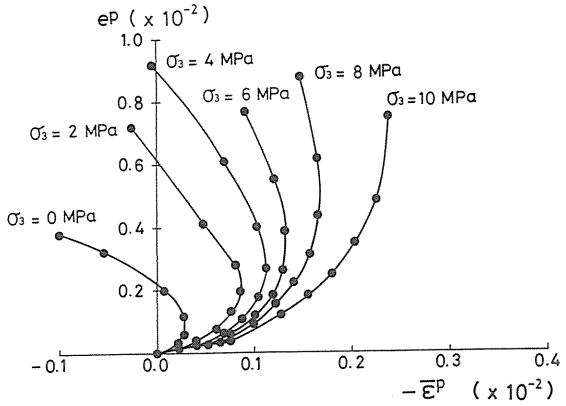

Fig. 5. 16. Deviatoric plastic strain-volumetoric plastic strain curves of Funyu-tuff for various confining pressures

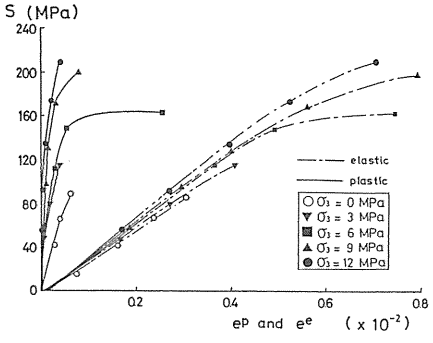

Fig. 5. 17. Deviatoric stress-volumetric elastic and plastic strain curves of Funyu-tuff for various confining pressures

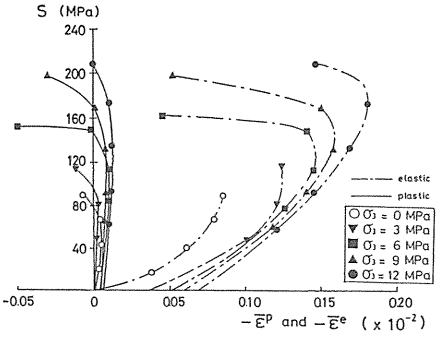

Fig. 5. 18. Deviatoric stress-deviatoric elastic and plastic strain curves of Funyu-tuff for various confining pressures

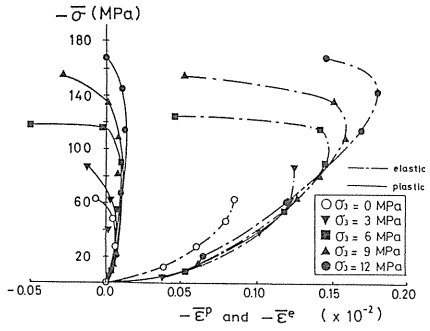

Fig. 5. 19. Volumetric stress-volumetric elastic and plastic strain curves of Funyu-tuff for various confining pressures

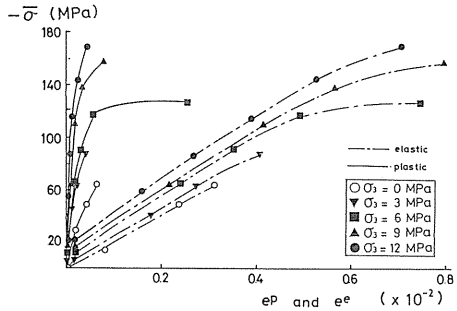

Fig. 5. 20. Volumetric stress-deviatoric elastic and plastic strain curves of Funyu-tuff for various confining pressures

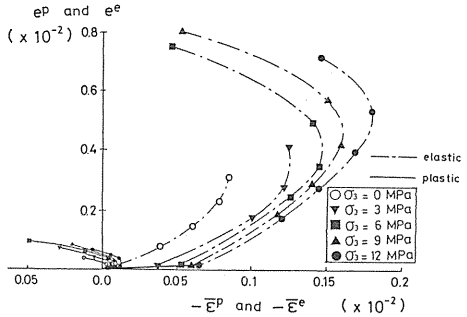

Fig. 5. 21. Deviatoric elastic and plastic strain-volumetric elastic and plastic strain curves of Funyu-tuff for various confining pressures

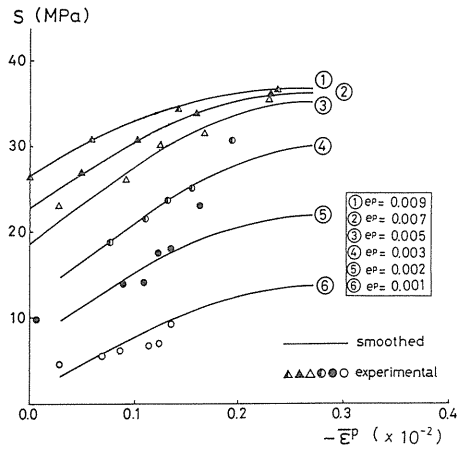

Fig. 5. 22. Smoothing of deviatoric stress-volumetric plastic strain response

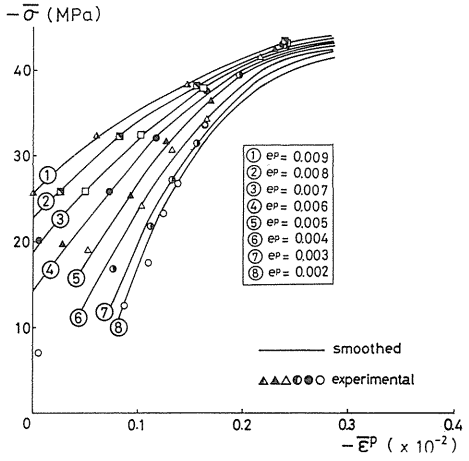

Fig. 5. 23. Smoothing of volumetric stress-volumetric plastic strain response

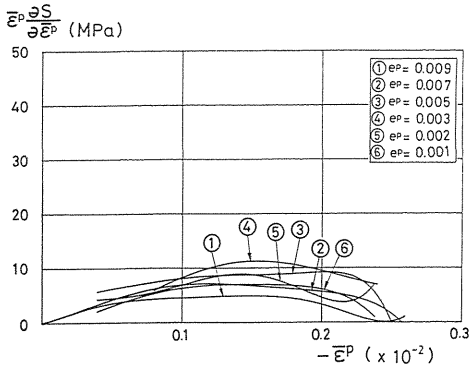

Fig. 5. 24. Plasticity spectra

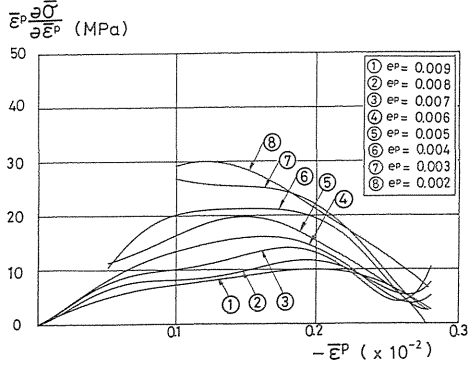

Fig. 5. 25. Plasticity spectra

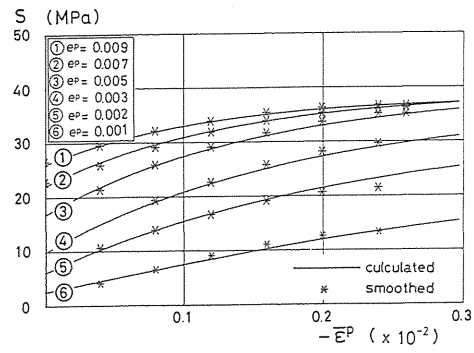

Fig. 5. 26. Calculated deviatoric response

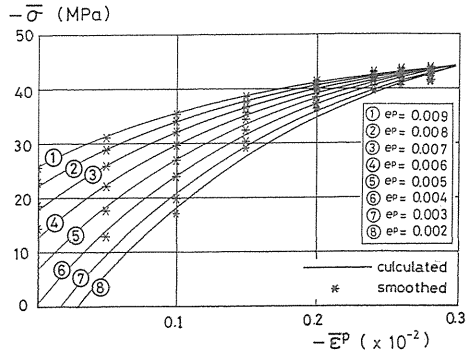

Fig. 5. 27. Calculated volumetric response

From Fig. 5.25, the values of volumetric response spectra points are:

$$\omega_{21}=0.00120,\ \tau_{21}=0.0020$$

$$\omega_{22}=0.00148,\ \tau_{22}=0.0040$$

The discretized plastic response functions are determined by the least square method as:

$$s=a_1\Gamma(e^p;\tau_{11})+a_2\Gamma(\bar{\varepsilon}^p;\omega_{11})+a_3\Gamma(e^p;\tau_{11})\Gamma(\bar{\varepsilon}^p;\omega_{11})$$
$$+a_4\Gamma(e^p;\tau_{12})+a_5\Gamma(\bar{\varepsilon}^p;\omega_{12})+a_6\Gamma(e^p;\tau_{12})\Gamma(\bar{\varepsilon}^p;\omega_{12}) \quad (70)$$

$$\bar{\sigma}=b_1\Gamma(e^p;\tau_{11})+b_2\Gamma(\bar{\varepsilon}^p;\omega_{11})+b_3\Gamma(e^p;\tau_{11})\Gamma(\bar{\varepsilon}^p;\omega_{11})$$
$$+b_4\Gamma(e^p;\tau_{12})+b_5\Gamma(\bar{\varepsilon}^p;\omega_{12})+b_6\Gamma(e^p;\tau_{12})\Gamma(\bar{\varepsilon}^p;\omega_{12}) \quad (71)$$

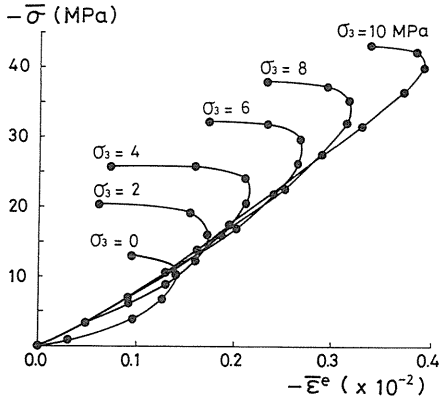

Fig. 5. 28. Volumetric stress-volumetric elastic strain curves of Funyu-tuff for various confining pressures

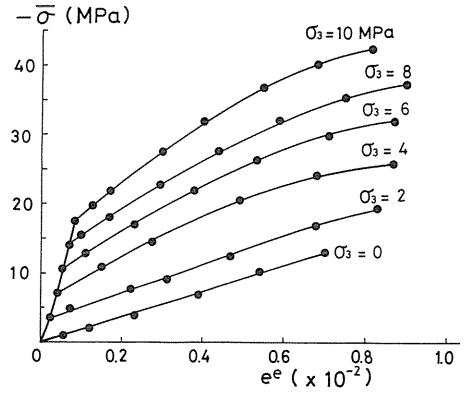

Fig. 5. 29. Volumetric stress-deviatoric elastic strain curves of Funyu-tuff for various confining pressures

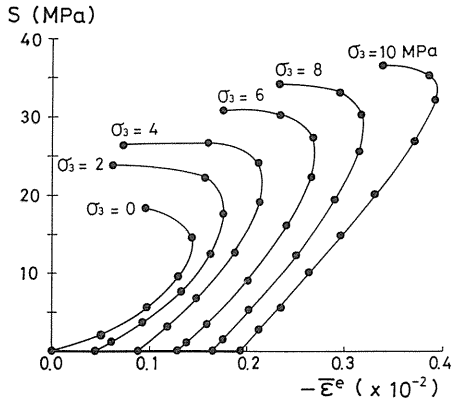

Fig. 5. 30. Deviatoric stress-volumetric elastic strain curves of Funyu-tuff for various confining pressures

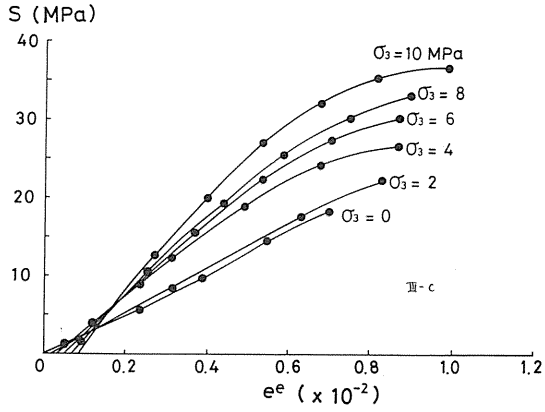

Fig. 5. 31. Deviatoric stress-deviatoric elastic strain curves of Funyu-tuff for various confining pressures

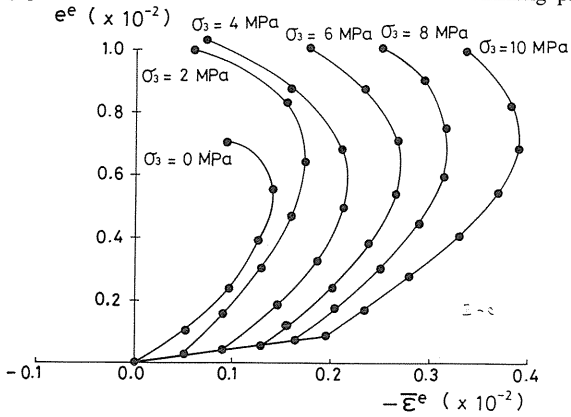

Fig. 5. 32. Deviatoric elastic strain-volumetric elastic strain curves of Funyu-tuff for various confining pressures

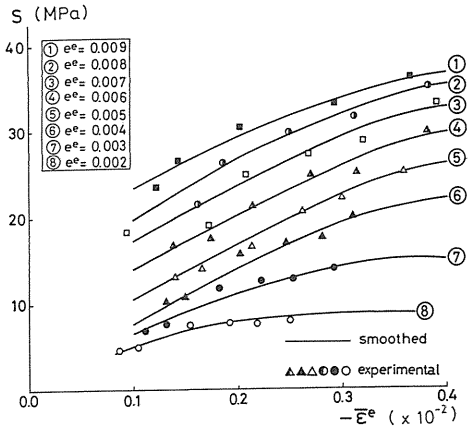

Fig. 5. 33. Smoothing of deviatoric stress-volumetric elastic strain response

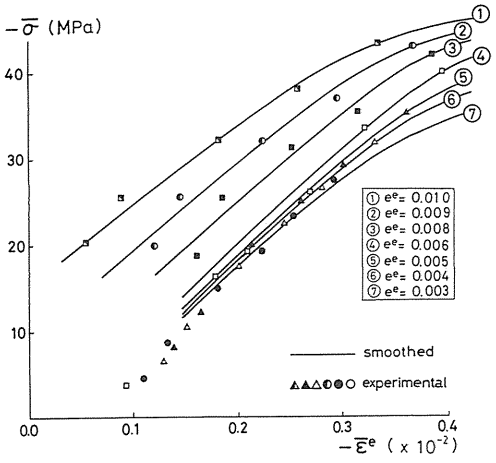

Fig. 5. 34. Smoothing of volumetric stress-volumetric elastic strain response

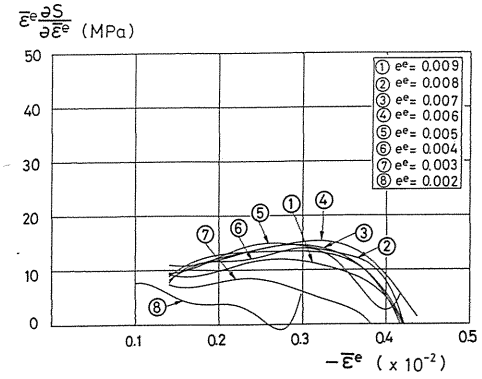

Fig. 5. 35. Elasticity spectra

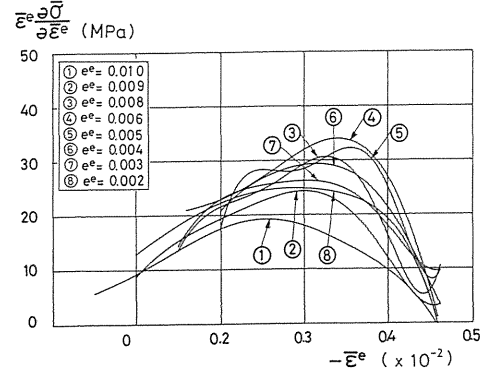

Fig. 5. 36. Elasticity spectra

where

$$a_1 = -17.327, \quad a_2 = -53.059, \quad a_3 = 74.139$$
$$a_4 = 51.727, \quad a_5 = 58.642, \quad a_6 = -80.756$$
$$b_1 = -106.747, \quad b_2 = -131.708, \quad b_3 = 119.261$$
$$b_4 = 146.965, \quad b_5 = 188.927, \quad b_6 = -171.312$$

The plotted plastic response functions are shown in Figs. 5.26 and 5.27.

5. 2. 2. Elastic response

Figs. 5.28 to 5.32 show the elastic responses for $(\bar{\sigma}-\bar{\varepsilon}^e)$, $(\bar{\sigma}-e^e)$, $(s-\bar{\varepsilon}^e)$, $(s-e^e)$ and $(e^e-\bar{\varepsilon}^e)$. Figs. 5.17 to 5.19 show the determined response function for $s(e^e,\bar{\varepsilon}^e)$ and $\bar{\sigma}(e^e-\bar{\varepsilon}^e)$. From these data, deviatoric stress s and volumetric stress $\bar{\sigma}$ given in Eqns. (41) and (42) are determined. As decribed in the previous section, following the smoothing procedure and the polynomial approximation, the calculated spectra of the elastic response functions are shown in Figs. 5.33 and 5.34. From Fig. 5.35, the values of deviatoric elastic response spectra points are:

$$\omega_{31}=0.00248,\quad \tau_{31}=0.0050$$

$$\omega_{32}=0.00325,\quad \tau_{32}=0.0060$$

From Fig. 5.36, the values of volumetric response spectra points are:

$$\omega_{41}=0.00352,\quad \tau_{41}=0.0050$$

$$\omega_{42}=0.00340,\quad \tau_{42}=0.0060$$

The discretized elastic response functions are determined by the least square method as:

$$s=c_1\Gamma(e^e;\tau_{31})+c_2\Gamma(\bar{\varepsilon}^e;\omega_{31})+c_3\Gamma(e^e;\tau_{31})\Gamma(\bar{\varepsilon}^e;\omega_{31})$$
$$+c_4\Gamma(e^e;\tau_{32})+c_5\Gamma(\bar{\varepsilon}^e;\omega_{32})+c_6\Gamma(e^e;\tau_{32})\Gamma(\bar{\varepsilon}^e;\omega_{32}) \tag{72}$$

$$\bar{\sigma}=d_1\Gamma(e^e;\tau_{41})+d_2\Gamma(\bar{\varepsilon}^3;\omega_{41})+d_3\Gamma(e^e;\tau_{41})\Gamma(\bar{\varepsilon}^e;\omega_{41})$$
$$d_4\Gamma(e^e;\tau_{42})+d_5\Gamma(\bar{\varepsilon}^e;\omega_{42})+d_6\Gamma(e^e;\tau_{42})\Gamma(\bar{\varepsilon}^e;\omega_{42}) \tag{73}$$

where

$$c_1=-182.541,\qquad c_2=-42.491,\qquad c_3=133.490$$

$$c_4=240.464,\qquad c_5=48.687,\qquad c_6=-106.899$$

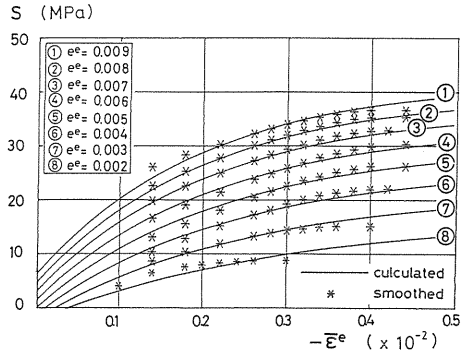

Fig. 5. 37. Calculated deviatoric response

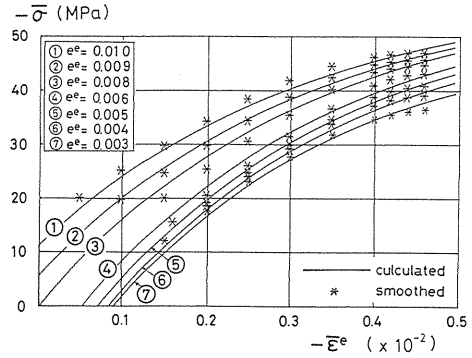

Fig. 5. 38. Calculated volumetric response

$$d_1=-788.448, \quad d_2=-912.203, \quad d_3=\ 972.646$$
$$d_4=\ 854.348, \quad d_5=\ 942.740, \quad d_6=-1015.690$$

The plotted elastic response functions are shown in Figs. 5.37 and 5.38.

5. 3. Elastic and plastic responses of granite

In this section, we describe the determined elastic and plastic response of granite which is a typical igneous rock.

5. 3. 1. Plastic response

Figs. 5.39 to 5.43 show the plastic responses for $(\bar{\sigma}-\bar{\varepsilon}^p)$, $(\bar{\sigma}-e^p)$, $(s-\bar{\varepsilon}^p)$, $(s-e^p)$ and $(e^p-\bar{\varepsilon}^p)$. Figs. 5.44 and 5.45 show the determined response function for $s(e^p,\bar{\varepsilon}^p)$ and $\bar{\sigma}(e^p-\bar{\varepsilon}^p)$. From these data, deviatoric stress s and volumetric stress $\bar{\sigma}$ given in Eqn. (30) are determined. As decribed in the previous section, following the smoothing procedure and the polynomial approximation, the calculated spectra of the plastic response functions are shown in Figs. 5.46 and 5.47. From Fig. 5.46, the values of deviatoric plastic response spectra points are:

$$\omega_{11}=0.000106, \quad \tau_{11}=0.0005$$
$$\omega_{12}=0.000900, \quad \tau_{12}=0.0003$$

From Fig. 5.47, the values of volumetric response spectra points are:

$$\omega_{21}=0.000119, \quad \tau_{21}=0.0003$$
$$\omega_{22}=0.000106, \quad \tau_{22}=0.0005$$

The discretized plastic response functions are determined by the least square method as:

$$s=a_1\Gamma(e^p;\tau_{11})+a_2\Gamma(\bar{\varepsilon}^p;\omega_{11})+a_3\Gamma(e^p;\tau_{11})\Gamma(\bar{\varepsilon}^p;\omega_{11})$$
$$+a_4\Gamma(e^p;\tau_{12})+a_5\Gamma(\bar{\varepsilon}^p;\omega_{12})+a_6\Gamma(e^p;\tau_{12})\Gamma(\bar{\varepsilon}^p;\omega_{12}) \tag{74}$$
$$\bar{\sigma}=b_1\Gamma(e^p;\tau_{11})+b_2\Gamma(\bar{\varepsilon}^p;\omega_{11})+b_3\Gamma(e^p;\tau_{11})\Gamma(\bar{\varepsilon}^p;\omega_{11})$$
$$+b_4\Gamma(e^p;\tau_{12})+b_5\Gamma(\bar{\varepsilon}^p;\omega_{12})+b_6(e^p;\tau_{12})\Gamma(\bar{\varepsilon};\omega_{12}) \tag{75}$$

where

$$a_1=\ 1699.882, \quad a_2=\ 264.563, \quad a_3=\ -273.128$$
$$a_4=-1207.729, \quad a_5=\ -689.785, \quad a_6=\ 1271.016$$
$$b_1=-1844.270, \quad b_2=-1391.040, \quad b_3=\ 2032.347$$
$$b_4=\ 2456.955, \quad b_5=\ 1443.098, \quad b_6=-2409.057$$

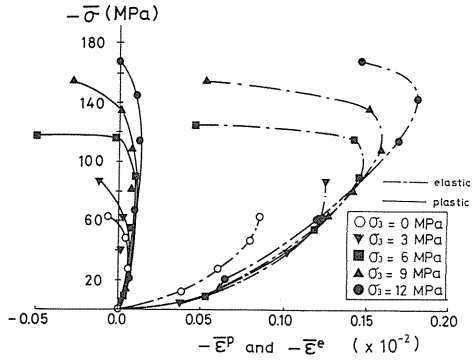

Fig. 5. 39. Volumetric stress-volumetric elastic and plastic strain curves of granite for various confining pressures

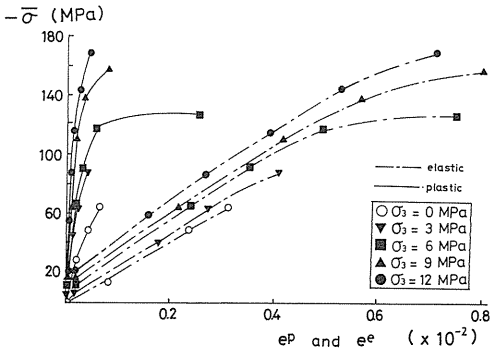

Fig. 5. 40. Volumetric stress-deviatoric elastic and plastic strain curves of granite for various confining pressures

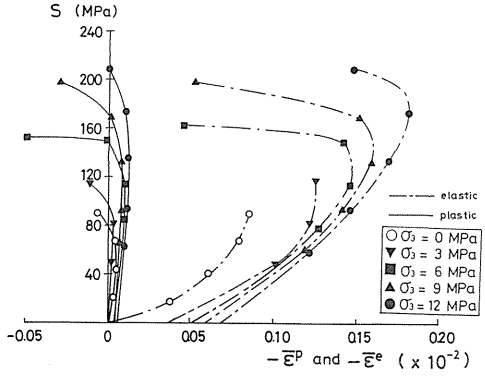

Fig. 5. 41. Deviatoric stress-volumetric elastic and plastic strain curves of granite for various confining pressures

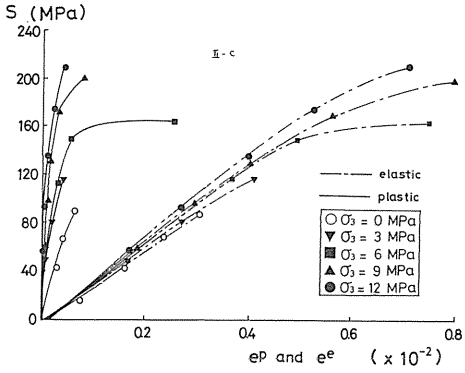

Fig. 5. 42. Deviatoric stress-deviatoric elastic and plastic strain curves of granite for various confining pressures

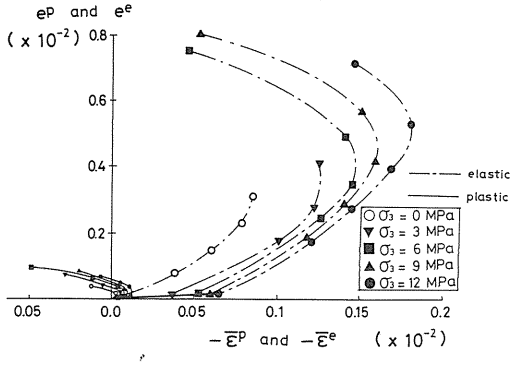

Fig. 5. 43. Deviatoric elastic and plastic strain-volumetric elastic and plastic strain curves of granite for various confining pressures

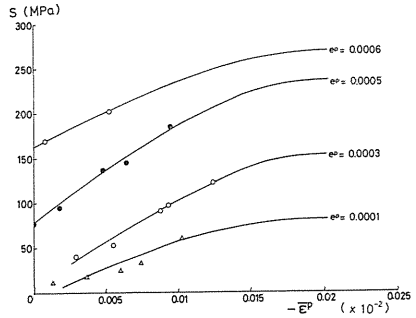

Fig. 5. 44. Smoothing of deviatoric stress-volumetric plastic strain response

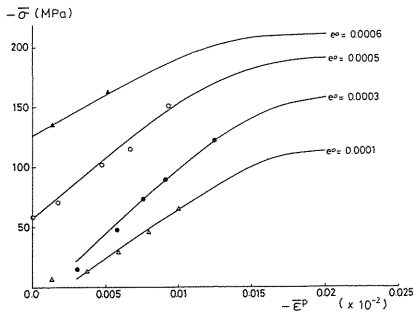

Fig. 5. 45. Smoothing of volumetric stress-volumetric plastic strain response

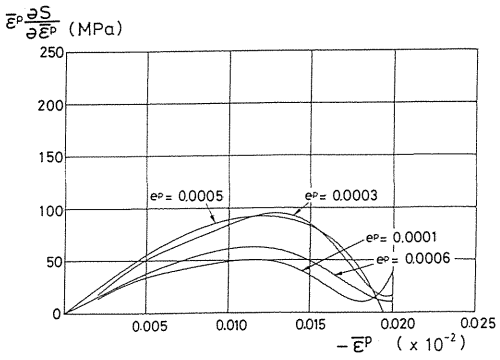

Fig. 5. 46. Plasticity spectra

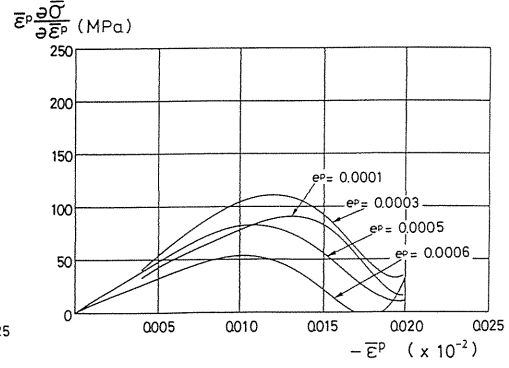

Fig. 5. 47. Plasticity spectra

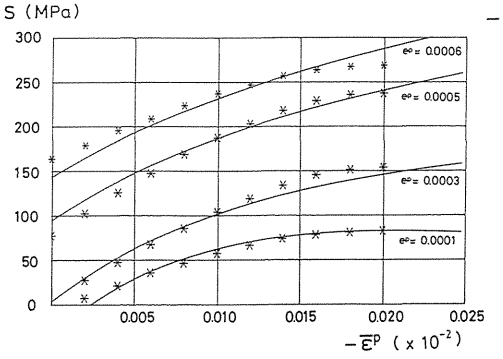

Fig. 5. 48. Calculated deviatoric response

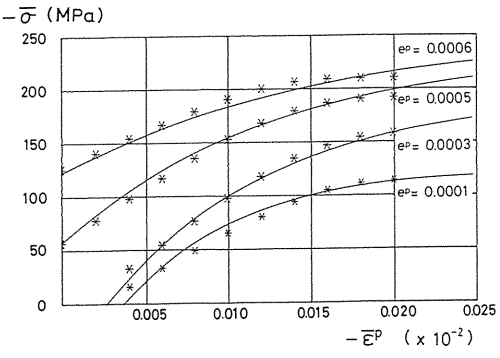

Fig. 5. 49. Calculated volumetric response

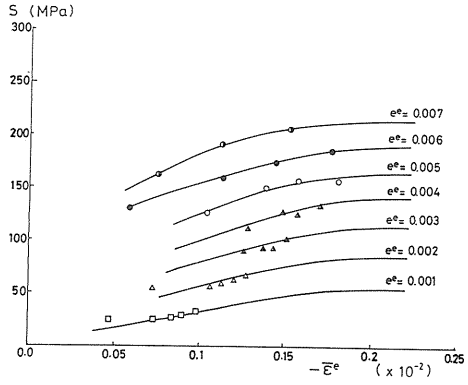

Fig. 5. 50. Smoothing of deviatoric stress-volumetric elastic strain response

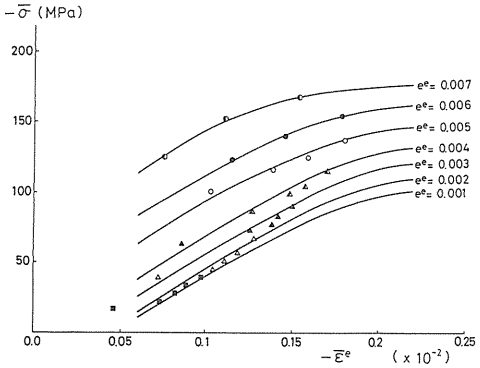

Fig. 5. 51. Smoothing of volumetric stress-volumetric elastic strain response

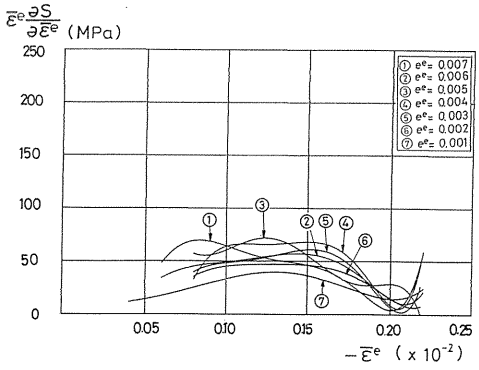

Fig. 5. 52. Elasticity spectra

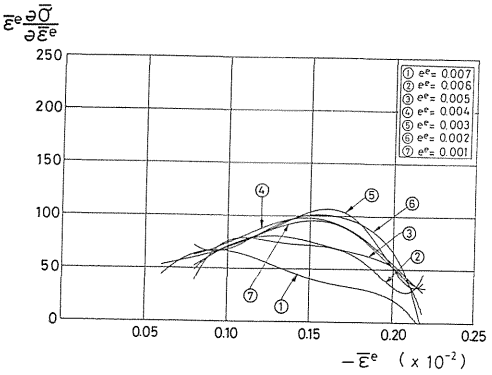

Fig. 5. 53. Elasticity spectra

The plotted plastic response functions are shown in Figs. 5.48 to 5.49.

5. 3. 2. *Elastic response*

Figs. 5.50 and 5.51 show the determined response function for $s(e^e, \bar{\varepsilon}^p)$ and $\bar{\sigma}(e^e - \bar{\varepsilon}^e)$. From these data, deviatoric stress s and volumetric stress $\bar{\sigma}$ given in Eqns. (41) and (42) are determined. As decribed in the previous section, following the smoothing procedure and the polynomial approximation, the calculated spectra of the elastic response functions are shown in Figs. 5.52 and 5.53. From Fig. 5.52, the values of deviatoric elastic response spectra points are:

$$\omega_{31}=0.001250,\ \tau_{31}=0.0050$$

$$\omega_{32}=0.001525,\ \tau_{32}=0.0040$$

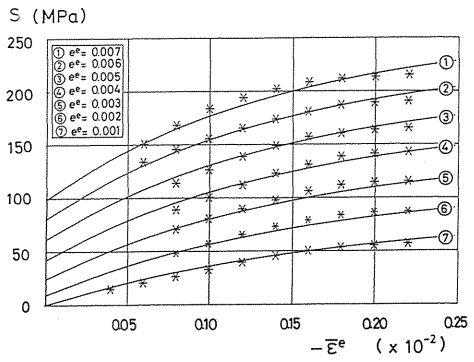

Fig. 5. 54. Calculated deviatoric response

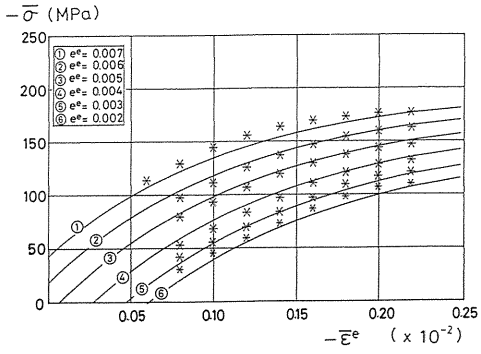

Fig. 5. 55. Calculated volumetric response

From Fig. 5.53, the values of volumetric response spectra points are:

$$\omega_{41}=0.001610,\quad \tau_{41}=0.0030$$

$$\omega_{42}=0.001550,\quad \tau_{42}=0.0020$$

The discretized elastic response functions are determined by the least square method as:

$$s=c_1\Gamma(e^e;\tau_{31})+c_1\Gamma(\bar{\varepsilon}^e;\omega_{31})+c_3\Gamma(e^e;\tau_{31})\Gamma(\bar{\varepsilon}^e;\omega_{31})$$
$$+c_4\Gamma(e^e;\tau_{32})+c_5\Gamma(\bar{\varepsilon}^e;\omega_{32})+c_6\Gamma(e^e;\tau_{32})\Gamma(\bar{\varepsilon}^e;\omega_{32}) \tag{76}$$

$$\sigma^-=d_1\Gamma(e^e;\tau_{41})+d_2\Gamma(\bar{\varepsilon}^e;\omega_{41})+d_3\Gamma(e^e;\tau_{41})\Gamma(\bar{\varepsilon}^e;\omega_{41})$$
$$+d_4\Gamma(e^e;\tau_{42})+d_5\Gamma(\bar{\varepsilon}^e;\omega_{42})+d_6\Gamma(e^e;\tau_{42})\Gamma(\bar{\varepsilon}^e;\omega_{42}) \tag{77}$$

where

$$c_1=\ 1296.597,\qquad c_2=\ -83.064,\qquad c_3=\ 136.694$$
$$c_4=-1062.887,\qquad c_5=\ 143.040,\qquad c_6=\ -3.733$$
$$d_1=\ 1171.019,\qquad d_2=-1030.365,\qquad d_3=-845.768$$
$$d_4=-1045.967,\qquad d_5=\ 1190.168,\qquad d_6=\ 772.034$$

The plotted elastic response functions are shown in Figs. 5.54 to 5.55.

6. Conclusions

As the volumetric deformation of geomaterials occurs independently of the shear deformation, the geomaterials can be said to be a general material as compared with the metals. Therefore, it is difficult to treat this kind of materials using the flow theory, more explicitly, the scalar potential theory. To solve the insufficiency of the flow theory, the multi-response theory has been proposed. Nevertheless, this theory requires very accurate measurements in order to determine the volumetric and deviatoric responses. In addition to this, a non-associated flow theory employing a dilatancy function has been presented. The responses and dilatancy functions are represented through the Laplace transformation. Then these model are applied to simulate the behaviour of several rocks under monotone and cyclic loadings. For the proposed theories, a procedure for triaxial tests of geomaterials by a stiff testing machine, a closed-measurement-analysis system for a laboratory test and a data bank system of rock triaxial test are described.

References

1) Drucker, D.C. & Prager, W. (1952): Soil mechanics and Plasticity Analysis on Limit Design, Quat. Applied Math., Vol.10, pp. 157–165.
2) Roscoe, K.H., Schofield, A.N. & Thurairajah, A. (1963): Yielding of Clay in State Wetter Than Critical, Geotechnique, Vol.13, No.3, pp. 211–240.
3) Lade, P.V. & Duncan, J.M. (1975): Elastoplastic Stress-Strain Theory for Cohesionless Soil, GT10, ASCE, pp. 1037–1053.
4) Sekiguchi, H. & Ohta, H. (1977): Induced Anisotropy and Time Dependency in Clays, Speciality Session 9, 9th Int. Conf. Soil Mech. Eng., pp. 229–239.
5) Rudnicki, J.W. & Rice, J.R. (1975): Conditions for the Localization of Deformation in Pressure-Sensitive Dilation Materials, J. Mech. Phys. Solids, Vol.23, pp. 371–394.
6) Ichikawa, Y., Kyoya, T. & Kawamoto, T. (1985): Incremental Theory of Plasticity for Rock, Procs. 5th Int. Conf. Numer. Meth. Geomechs., Vol.1, pp. 451–462.
7) Mroz, Z. (1967): On The Description on Anisotropic Workhardening, J. Mech. Phy. Solids, Vol.15, pp. 163–175.
8) Prevost, J.H. (1977): Mathematical Modelling of Monotonic and Cyclic Undrained Clay Behaviour, Int. J. Numer. Anal. Methods Geomech., Vol.1, pp. 159–216.
9) Prevost, J.H. (1978): Plasticity Theory for Soil Stress-Strain Behaviour, EM104, ASCE, pp. 1177–1194.
10) Mroz, Z., Norris, V.A. & Zienkiewicz, O.C. (1978): An Anisotropic Hardening Model for Soils and its Application to Cyclic Loading, Int. J. Numer. Anal. Meth. Geomech., Vol.2, pp. 203–221.
11) Dafalias, Y.F. & Herrmann, L.R. (1982): Boundary Surface Formulation of Soil Plasticity, in Soil Mechanics-Transcient and Cyclic Loads, ed. by G.N. Pande & O.C. Zienkiewicz, John Wiley, pp. 253–282.
12) Ichikawa, Y., Kyoya, T. & Kawamoto, T. (1988): Incremental Theory of Elasticity and Plasticity under Cyclic Loading, Procs. 6th Int. Conf. Num. Meth. Geomechs., Vol.1, pp. 327–334.
13) Kawamoto, T., Tokashiki, N. & Ishizuka, Y. (1981): On Uniaxial Compression Test of Rock-Like Materials Using a New Type of High Stiff Testing Machine (Japanese), J. Soc. Mater. Sci., Vol.30, No.332, pp. 517–523.